

Online Experimental Design for Network Tomography

Xuchuang Wang¹, Yu-Zhen Janice Chen¹, Matheus Guedes de Andrade¹
Mohammad Hajiesmaili¹, John C.S. Lui², Ting He³, Don Towsley¹

¹*University of Massachusetts, Amherst, MA*

²*Chinese University of Hong Kong, Hong Kong*

³*Pennsylvania State University, University Park, PA*

Abstract

How to efficiently perform network tomography is a fundamental problem in network management and monitoring. A network tomography task usually consists of applying multiple probing experiments, e.g., across different paths or via different casts (including unicast and multicast). We study how to optimize the network tomography process through online sequential decision-making. From the methodology perspective, we introduce an online probe allocation algorithm that dynamically performs network tomography based on the principles of optimal experimental design and the maximum likelihood estimation. We rigorously analyze the regret of the algorithm under the conditions that *i*) the optimal allocation is Lipschitz continuous in the parameters being estimated and *ii*) the parameter estimators satisfy a concentration property. From the application perspective, we present two case studies: *a*) the classical lossy packet-switched network and *b*) the quantum bit-flip network. We show that both cases fulfill the two theoretical conditions and provide their corresponding regrets when deploying our proposed online probe allocation algorithm. Besides these two case studies with theoretical guarantees, we also conduct simulations to compare our proposed algorithm with existing methods and demonstrate our algorithm's effectiveness in a broader range of scenarios.

1 Introduction

Network tomography [Coates et al., 2002, He et al., 2021, De Andrade et al., 2023] is an essential approach for inferring the internal network (e.g., link) parameters, such as the loss rate, delay, and bandwidth, via end-to-end (external) measurements. These external measurements are practically more accessible than the network's internal components (e.g., routers), which may be owned by different internet service providers (ISPs) [Cáceres et al., 1999] and are difficult to access. A stochastic network tomography problem consists of a network with

a set \mathcal{L} of $L := |\mathcal{L}|$ links, each link $\ell \in \mathcal{L}$ with an unknown parameter μ_ℓ that characterizes its stochastic property (e.g., μ_ℓ may represent loss rate or average delay of the link), and a set \mathcal{M} of $M := |\mathcal{M}|$ probes. Performing a probe on the network refers to generating one or multiple stochastic measurements (i.e., *observations*) that depend on the network parameters. Network tomography aims to estimate the network parameters μ_ℓ from the observations.

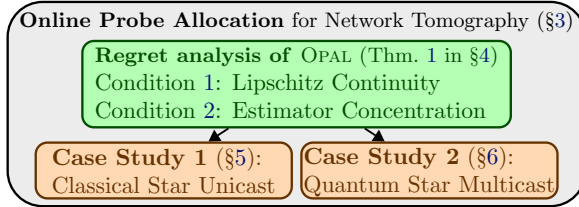
Most prior works on network tomography focus on devising estimators for the network parameters from the stochastic observations, e.g., in packet delay tomography [Duffield and Lo Presti, 2000, Lo Presti et al., 2002, Gu et al., 2010] and loss network tomography [Cáceres et al., 1999, Xi et al., 2006] (detailed related works are in Section 1.2). That is, after obtaining these stochastic observations from probes, prior works aim to devise good *static* estimators to infer the network parameters. While the static estimator design is crucial for network tomography, another essential yet less explored task is, without knowing the network parameters $(\mu_\ell)_{\ell \in \mathcal{L}}$, how to *dynamically* collect online observations to *efficiently* estimate the network parameters using the least number of probes. In short, this is a sequential decision-making problem (a.k.a., online learning) [Barto et al., 1989] for network tomography.

However, to apply online learning techniques to network tomography, one needs to tackle unique challenges not present in common online learning scenarios. A key technical challenge comes from the complex feedback mechanism in network tomography. In standard online learning settings, e.g., basic multi-armed bandits [Auer, 2002] or linear bandits [Li et al., 2010], the feedback is usually a scalar stochastic reward or loss, which is only related to the action (probe) taken by the algorithm. In contrast, in network tomography, feedback consists of the stochastic observations (e.g., a random vector) generated by the probes via the compound effect of the links across a set of paths traversed by the probe. The observations often have a non-linear relation with the network parameters, which may correlate with each other, making the combinatorial bandits framework [Chen et al., 2013] difficult to apply. This complex feedback mechanism makes the design of the online algorithm and the analysis of its regret challenging.

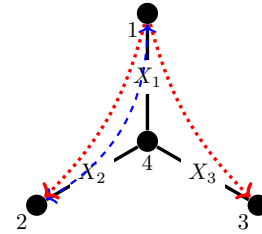
1.1 Contributions

In this paper, we consider the network tomography task as an online sequential decision making problem and focus on two new perspectives: (1) A general framework that allows us to handle both classical and quantum network tomography tasks [De Andrade et al., 2022, 2023]. (2) Fine-grained analysis, where we develop new algorithms to perform online network tomography with regret guarantees. More specifically, this paper makes the following contributions:

- First, we formulate a general network tomography task as an online experimental design problem (Section 2). One attractive feature of this general model is that it covers both classical and quantum tomography scenarios. The problem of adaptively collecting probe observations and efficiently inferring the network parameters is formulated as a *regret* minimization problem, where the



(a) Paper Structure



(b) 3-Link Star Network

Figure 1: (a) A schematic diagram of the paper structure. We identify two conditions to analyze the regret of the greedy dynamic network tomography algorithm. These conditions are validated through two case studies: the classical loss star network tomography and the quantum star network tomography. (b) A star network with 4 nodes: Denote the central node as 4, and the peripheral nodes are denoted as 1, 2, 3. The solid lines represent the loss characteristics of the network (modeled by Bernoulli random variables X_1, X_2, X_3), the dashed blue line represents a unicast probe (probe at node 1, receive at node 2, or vice versa), and the two dotted red lines represent a multicast probe (probe at node 1, duplicate at intermediate node 4, receive at nodes 2 and 3).

objective is to minimize the difference between the performance of an online algorithm and the optimal policy in terms of optimal experimental design (OED) criteria [Pukelsheim, 2006]. To our knowledge, this paper is the first to design network tomography algorithms for the purpose of minimizing regret.

► Second, we devise the Online Probe Allocation (OPAL) algorithm for the general network tomography task (Section 3). The design of this algorithm is inspired by the idea of “chasing optimal bounds,” which is the backbone for a class of online learning algorithms with optimal performance [Garivier and Kaufmann, 2016, Combes et al., 2017]. We refer to the actual probe allocation ratio of the algorithm as *actual allocation* and the optimal allocation ratio based on the estimated network parameters as *estimated optimal allocation*. OPAL uses the difference between the actual allocation and the estimated optimal allocation to direct the algorithm to sequentially sample the most inadequately performed probes.

► Third, we propose a new analysis framework for studying the regret of OPAL (Section 4). Analyzing the regret of OPAL is challenging: The chased estimated optimal allocation varies over time (determined by the estimated network parameters), whose accuracy is also affected by the probing decisions. Furthermore, the online algorithm’s actual allocation depends on all its past probe decisions, which lags behind the time-varying estimated optimal allocation it chases. We propose two critical conditions (Section 4.1): *Lipschitz continuity* (Condition 1) and *confidence interval concentration* (Condition 2), that abstract the property of any network tomography task. With these two theoretical conditions, we then rigorously prove that OPAL achieves a $\tilde{O}((\xi T)^{-\gamma_{\min}} +$

$\xi \mathbb{1}\{\exists m \in \mathcal{M} : \phi_m^* < \xi\}$ regret (convergence rate), where T is the total number of probes, $\gamma_{\min} \in (0, 1/2)$ is the smallest concentration rate of Condition 2, $\xi \in (0, 1)$ is an input constant of OPAL, $\mathbb{1}\{\cdot\}$ is an indicator function, ϕ_m^* is the optimal allocation ratio of the m -th probe, and the $\tilde{O}(\cdot)$ notation hides poly-logarithmic $\log T$ terms. While one can simply set $\xi = T^{-\gamma_{\min}/(1+\gamma_{\min})}$ to maintain a worst-case $\tilde{O}(T^{-\gamma_{\min}/(1+\gamma_{\min})})$ regret, in scenarios with a positive lower bound for ϕ_m^* of all probes, the second term can be set to 0 by a constant ξ , yielding a $\tilde{O}(T^{-\gamma_{\min}})$ regret.

► Last but not least, we present two case studies on classical and quantum networks to demonstrate the effectiveness of our proposed framework and algorithms from both theoretical and empirical aspects (Sections 5 and 6). For *classical network tomography* (Section 5), we first consider loss tomography in a classical star network with unicast probes and verify that the two theoretical conditions in our analysis framework are indeed satisfied in this tomography task, providing a $\tilde{O}(T^{-1/2})$ regret of OPAL for this classical tomography task (Section 5.1). Then, we conduct extensive experiments to corroborate the empirical performance of OPAL in classical network tomography (Section 5.2). For *quantum network tomography* (Section 6), we verify the two theoretical conditions for the bit-flip channel tomography in quantum star network with multicast probes and prove a $\tilde{O}(T^{-1/3})$ regret for this quantum tomography task (Section 6.1). Finally, we provide the empirical results of OPAL in this quantum network tomography task (Section 6.2) and show that OPAL outperforms alternative baseline policies. The main structure of this paper is illustrated in Figure 1a.

1.2 Related Works

Network tomography has been studied for decades [Cáceres et al., 1999, Duffield and Lo Presti, 2000, Lo Presti et al., 2002, Coates et al., 2002, Bu et al., 2002, Tsang et al., 2003, Xi et al., 2006, Gu et al., 2010, Gopalan and Ramasubramanian, 2011, Ma et al., 2014, He et al., 2015, De Andrade et al., 2022, 2023], and most prior works focus on the estimation of network parameters. For example, for the delay network tomography [Tsang et al., 2003], Lo Presti et al. [2002], Gu et al. [2010] study the estimator design for unicast probes, and Duffield and Lo Presti [2000] study the multicast probes. For loss network tomography, Cáceres et al. [1999] devise the maximum likelihood estimators, and Xi et al. [2006] propose EM-based estimations, both of which are for multicast probes. Recently, network tomography in quantum networks is studied by De Andrade et al. [2022, 2023], where, due to the complexity of the quantum network and information, only multicast probes on the quantum star network are considered. The estimators and probes studied in these previous form a solid foundation for our study from the online experimental design perspective. But, as our work focuses on the sequential probe selection and theoretical guarantees, the existing works are not directly applicable to our study.

Optimal experimental design (OED) is an approach to designing experiments to achieve specific statistical criteria [Pukelsheim, 2006]. It has been applied

in a wide range of applications, including clinical trial [Haines et al., 2003], synthetic biology [Gilman et al., 2021], and chemistry [Leardi, 2009], etc. The OED for network tomography is also studied, He et al. [2015], Kveton et al. [2022], Gu et al. [2010], Xi et al. [2006], to name a few. Among them, the most related work to this paper is He et al. [2015], where they proposed a heuristic iterative algorithm in terms of OED for the unicast network tomography task, and only an asymptotic convergence guarantee is provided. In this paper, we make a concrete step forward by proposing a rigorous *online* experimental design algorithm, OPAL, for network tomography, and we are the *first* to provide a fine-grained regret analysis for the network tomography task. Outside the network tomography literature, online experimental design for linear regression is studied by Fontaine et al. [2021], Allen-Zhu et al. [2021]. However, the linear regression model is too simple to apply to network tomography, whose feedback can be non-linear and correlated.

Online experimental design is closely related to online learning (a.k.a., sequential decision making), both of which aim to optimize the sequence of decisions (performed probes) in terms of possibly different objectives. Online learning is a fundamental model in machine learning and statistics [Hazan et al., 2016, Lattimore and Szepesvári, 2020], which typically consists of a learner repeatedly making decisions, observing the outcomes, and updating its decision-making policy based on the observed outcomes. Online learning algorithms have been applied to various fields, such as recommendation systems [Li et al., 2010], social influence maximization [Chen et al., 2009], and shortest path routing [Fu and Modiano, 2022]. While the high-level idea of online learning may have appeared in the network tomography literature, e.g., heuristically in He et al. [2015], this work is the first to propose a rigorous online experimental design algorithm as well as the theoretical analysis of the regret for the network tomography task. On the other hand, while many powerful algorithms in online learning have been proposed, e.g., upper confidence bound (UCB) [Auer, 2002], Thompson sampling [Thompson, 1933], these algorithms are not directly applicable to network tomography due to the complex structure between the network parameters and the probe observations, and we are the first to study the online experimental design algorithm in the network tomography problem.

2 Modeling and Formulation

In this section, we first formulate the general network tomography problem in Section 2.1 and then present the classical loss and quantum bit-flip network tomography problems in Sections 2.2 and 2.3, respectively, to further elaborate on the tomography tasks. Preliminaries of the optimal experimental design are introduced in Section 2.4. Lastly, we cast the network tomography problem as an online experimental design problem in Section 2.5.

2.1 General Network Tomography

Denote $\mathcal{G} = (\mathcal{N}, \mathcal{L})$ as a network topology with a set of $N \in \mathbb{N}^+$ nodes $\mathcal{N} := \{1, 2, \dots, N\}$ and a set of $L \in \mathbb{N}^+$ links $\mathcal{L} := \{1, 2, \dots, L\}$. Each link $\ell \in \mathcal{L}$ is associated with a stochastic model X_ℓ representing the characteristic of the link, e.g., a Bernoulli random variable for signal loss [Cáceres et al., 1999], or a Gaussian random variable for the packet delay variation (PDV) [Tsang et al., 2003], or the noise level or fidelity for quantum channel [Nielsen and Chuang, 2010]. We refer to a connection between two nodes (source and destination) across several consecutive links as a *path* in the network. The tomography task assumes that the link model is known, but that its parameters, denoted as a vector $\boldsymbol{\mu} := (\mu_\ell)_{\ell \in \mathcal{L}}$ (e.g., the link success rates), are unknown.

The network tomography task aims to estimate these unknown link parameters via a given set of $M \in \mathbb{N}^+$ probing experiments $\mathcal{M} := \{1, 2, \dots, M\}$ (called *probes* later), examples of which are unicast [He et al., 2015] and multicast [Cáceres et al., 1999]. Each probe $m \in \mathcal{M}$ is associated with one path or a set of paths consisting of one source node (sender) and a set of destination nodes (receivers) denoted as $\mathcal{N}_m \subseteq \mathcal{N}$ (see Figure 1b for an example), and the feedback $\mathbf{Y}_m \in \mathbb{R}^{|\mathcal{N}_m|}$ from the probing experiment m consists of received signals at the destination nodes in \mathcal{N}_m . Denote the probability of observing feedback \mathbf{Y}_m given network parameters $\boldsymbol{\mu}$ and probing experiment m as $f_m(\mathbf{Y}_m; \boldsymbol{\mu})$. The goal is to estimate the network parameters based on the feedback from the probing experiments. For ease of presentation, we follow the common identifiability assumption in network tomography literature [Bu et al., 2002, He et al., 2015] that the network parameters $\boldsymbol{\mu}$ can be uniquely determined from the feedback of sufficiently many probing experiments in \mathcal{M} . Given a set of $T \in \mathbb{N}^+$ probe-feedback pairs $\mathcal{H} := \{(m_t, \mathbf{Y}_{m_t, t})\}_{t=1}^T$, we define the log-likelihood function as $L(\boldsymbol{\mu}; \mathcal{H}) := \sum_{t=1}^T \log f_{m_t}(\mathbf{Y}_{m_t, t}; \boldsymbol{\mu})$. The maximum likelihood estimation (MLE) estimator for the network parameters $\boldsymbol{\mu}$ is defined as $\text{MLE}(\mathcal{H}) := \arg \max_{\boldsymbol{\mu}} L(\boldsymbol{\mu}; \mathcal{H})$.¹

Next, we use classical loss network tomography (Section 2.2) and quantum bit-flip network tomography (Section 2.3) as examples to illustrate the network tomography model in more detail.

2.2 Classical Loss Network Tomography

In a loss network, associated with each link $\ell \in \mathcal{L}$ is a Bernoulli random variable $X_\ell \sim \mathcal{B}(\mu_\ell)$ representing loss on that link, where $\mu_\ell \in (0, 1)$ is the probability that a transmitted signal is *not* lost, i.e., $\mathbb{P}(X_\ell = 1) = \mu_\ell$. We assume all these Bernoulli random variables are independent across links and time. As an example, a star loss network with $N = 4$ nodes and $L = 3$ links is depicted in Figure 1b. Later in Section 5, we further theoretically and empirically investigate this model.

¹Throughout this paper, we assume the outputs of the arg min and arg max functions are unique; otherwise, one can break the tie arbitrarily.

Unicast [He et al., 2015] and multicast [Cáceres et al., 1999] are two common probes in the loss networks. To elaborate on their details, let us consider the star network in Figure 1b and focus on end-to-end tomography where one only has access to the peripheral nodes 1, 2, 3, including sending signals to any other peripheral nodes and receiving signals sent from other end nodes. The unicast probe refers to sending signals across one path from one source node to one destination node, and the multicast probe refers to sending a signal from one source node down through a tree to multiple destination nodes, where the signal is duplicated at bifurcation nodes within the tree. For example, in Figure 1b, the dashed blue arrow between nodes 1 and 2 represents a unicast probe, where one can send signals from node 1, across central node 4, and then receive them at node 2 or vice versa from node 2 to node 1, denoted as $(1 \leftrightarrow 2)$ since the unicast probe is *symmetric*. The probability of receiving signals at node 2 when sending signals from node 1 is $f_{m=(1 \leftrightarrow 2)}(\mathbf{Y}_m = 1; \boldsymbol{\mu}) = \mathbb{P}(X_1 X_2 = 1) = \mu_1 \mu_2$. In this 3-link star network, there are in total three unicast probes: $(1 \leftrightarrow 2)$, $(1 \leftrightarrow 3)$, $(2 \leftrightarrow 3)$. The two dotted red arrows in Figure 1b together represent a multicast probe. Here node 1 is the source node and send signals to nodes 2 and 3. Then, the probability of receiving signals at both nodes 2 and 3 is $f_{m=(1 \rightarrow (2,3))}(\mathbf{Y}_m = (1, 1); \boldsymbol{\mu}) = \mathbb{P}(X_1 X_2 = 1, X_1 X_3 = 1) = \mu_1 \mu_2 \mu_3$, and the probability of receiving signals at node 2 but not at node 3 is $f_{m=(1 \rightarrow (2,3))}(\mathbf{Y}_m = (1, 0); \boldsymbol{\mu}) = \mathbb{P}(X_1 X_2 = 1, X_1 X_3 = 0) = \mu_1 \mu_2 (1 - \mu_3)$, and so on. Using the feedback from the unicast and multicast probes, one can infer the loss characteristics of all links—the parameters μ_1, μ_2, μ_3 of the star network in Figure 1b.

2.3 Quantum Bit-flip Network Tomography

Background of General quantum network tomography Quantum networks are communication systems formed by the interconnection of quantum processors. Despite the stark difference between the physical properties of classical and quantum information systems, network tomography extends naturally to the quantum setting. Similar to the classical case of learning link parameters, quantum network tomography addresses the characterization of quantum channels representing links in a quantum network through end-to-end measurements [De Andrade et al., 2024]. Quantum network tomography is defined under the assumption that the quantum channel representing link $\ell \in \mathcal{L}$, has the parametric form $\mathcal{E}(\rho) = \sum_k M_{\ell k}^\dagger(\mu_\ell) \rho M_{\ell k}(\mu_\ell)$, where $\mu_\ell \in \mathbb{R}^{d_\ell}$ for $d_\ell \in \mathbb{N}^+$ are the parameters, ρ is an input state, $\{M_{\ell k}\}$ denote the Kraus operators for \mathcal{E}_ℓ . The goal of quantum network tomography is to estimate μ_ℓ for each link $\ell \in \mathcal{L}$.

Quantum network tomography probes consist of (a) a quantum algorithm for the distribution of quantum states in the network and (b) quantum measurement operators performed in the end nodes for each distributed state. The algorithm for state distribution simultaneously specifies which links and intermediate node operations are used for distribution. Like the classical case, the output of quantum measurements performed in the end nodes yields a random vector \mathbf{Y}_m whose statistics depend on network parameters $\boldsymbol{\mu}$.

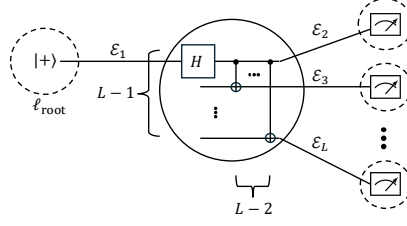


Figure 2: Root independent multicast for quantum star network tomography. The root $\ell_{\text{root}} = 1$ prepares state $|+\rangle$, transmits it to the central node, and an $(L - 1)$ qubit state is prepared from the application of CNOT gates. Each output is transmitted to an end node via the links representing the quantum channels \mathcal{E}_ℓ , for $\ell = 2, \dots, L$. \mathbf{P}_Z basis measurements performed in the end nodes generate boolean random variables $\mathbf{Y}_{\ell_{\text{root}}} \in \{0, 1\}^{L-1}$.

Quantum bit-flip network tomography In this work, we apply our online experimental design algorithm to optimize the quantum network tomography of bit-flip channels in quantum networks with star topology [De Andrade et al. \[2022, 2023\]](#). Quantum network links are assumed to be *single-qubit, bit-flip* channels of the form $\mathcal{E}(\rho) = \mu_\ell \rho + (1 - \mu_\ell) \mathbf{P}_X \rho \mathbf{P}_X$, where $\mu_\ell \in (0, 1)$ denotes the probability of no bit-flip for link $\ell \in \mathcal{L}$, and \mathbf{P}_X is the Pauli X operator [Nielsen and Chuang \[2010\]](#). We utilize probes defined in [De Andrade et al. \[2023\]](#) that rely on multipartite quantum state distribution, focusing on the *Root Independent* distribution strategy depicted in Fig 2, which we now describe. The number of nodes N in the star network equals the number of links L plus one, i.e., $N = L + 1$. The process starts with the selection of a root node (link) ℓ_{root} , which sends a qubit in state $|+\rangle$ to the intermediate node.² Upon receiving the qubit from ℓ_{root} , the intermediate node applies a Hadamard gate [Nielsen and Chuang \[2010\]](#) in the qubit and performs an $(L - 1)$ -qubit CNOT gate on $(L - 2)$ ancilla qubits initialized in state $|0\rangle$ controlled by the received qubit. Each output of the CNOT gate is sent to the end nodes of the star, excluding ℓ_{root} , such that an $(L - 1)$ -qubit quantum state is prepared in the rest $(L - 1)$ end nodes. The process terminates with \mathbf{P}_Z -basis measurements performed on the qubits received by the end nodes. The probability of observing a $|b_2 b_3 \dots b_L\rangle$ quantum state (for $b_\ell \in \{0, 1\}$) at the $L - 1$ end nodes after sending $|+\rangle$ at node $\ell_{\text{root}} = 1$ is $f_{m=1}(Y_m = |b_2 b_3 \dots b_L\rangle; \boldsymbol{\mu}) = \prod_{\ell=2}^L \mu_\ell^{b_\ell} (1 - \mu_\ell)^{1-b_\ell}$. The online experimental design algorithm can be applied to different quantum network tomography probes, such as the additional multipartite probes defined in [De Andrade et al. \[2023\]](#). Later, we provide a detailed case study of applying our new algorithm to this quantum bit-flip network tomography model in Section 6.

²We use Dirac notation for quantum states sparingly in this paper, such as, $|+\rangle$ and $|0\rangle$, for rigor. However, understanding these notations is not necessary for following the content. We refer interested readers to [Nielsen and Chuang \[2010\]](#).

2.4 Preliminaries of Optimal Experimental Design

Fisher Information Matrix and Cramér-Rao Bound The Fisher information matrix (FIM) of probing the network via the probe $m \in \mathcal{M}$ with respect to the link parameters $\boldsymbol{\mu}$ is defined as follows,

$$\mathbf{I}_m(\boldsymbol{\mu}) := \left(\mathbb{E}_{\mathbf{Y}_m} \left[\frac{\partial \log f_m(\mathbf{Y}_m; \boldsymbol{\mu})}{\partial \mu_\ell} \frac{\partial \log f_m(\mathbf{Y}_m; \boldsymbol{\mu})}{\partial \mu_{\ell'}} \middle| \boldsymbol{\mu} \right] \right)_{(\ell, \ell') \in \mathcal{L} \times \mathcal{L}}.$$

We denote $\boldsymbol{\phi} \in \Delta^{M-1}$ as the allocation ratio (probability distribution) of the number of times of each of the M probes S_m over the total number of times of performing probes $\sum_{m \in \mathcal{M}} S_m$, where Δ^{M-1} is the probability simplex in \mathbb{R}^M . Denote $\mathbf{I}(\boldsymbol{\mu}; \boldsymbol{\phi})$ as the FIM of probing the network via the mixture of multiple probes according to an allocation $\boldsymbol{\phi}$ with respect to the network parameters $\boldsymbol{\mu}$. With the linearity of FIM, we have $\mathbf{I}(\boldsymbol{\mu}; \boldsymbol{\phi}) = \sum_{m=1}^M \phi_m \mathbf{I}_m(\boldsymbol{\mu})$. The Cramér-Rao bound (CRB) states that the covariance matrix of any unbiased estimator $\hat{\boldsymbol{\mu}} := (\hat{\mu}_\ell)_{\ell \in \mathcal{L}}$ of the network parameters $\boldsymbol{\mu}$ (under allocation $\boldsymbol{\phi}$) is lower bounded by the inverse of the FIM, i.e., $\text{Cov}(\hat{\boldsymbol{\mu}}) \succcurlyeq \mathbf{I}^{-1}(\boldsymbol{\mu}; \boldsymbol{\phi})$ [Lehmann and Casella, 2006], where $\mathbf{A} \succcurlyeq \mathbf{B}$ denotes that $\mathbf{A} - \mathbf{B}$ is a positive semi-definite matrix. In particular, when the MLE estimator $\hat{\boldsymbol{\mu}}_{\text{MLE}}$ is unbiased, it achieves the CRB, i.e., $\text{Cov}(\hat{\boldsymbol{\mu}}_{\text{MLE}}) = \mathbf{I}^{-1}(\boldsymbol{\mu}; \boldsymbol{\phi})$. Picking the trace of the matrices on both sides of the CRB yields that the mean square error (MSE) of the unbiased estimator $\hat{\boldsymbol{\mu}}$ is lower bounded by the trace of the inverse of the FIM, i.e., $\mathbb{E}[\|\hat{\boldsymbol{\mu}} - \boldsymbol{\mu}\|^2] \geq \text{tr}(\mathbf{I}^{-1}(\boldsymbol{\mu}; \boldsymbol{\phi}))$. In addition to the MSE, this estimation accuracy can be measured from many different perspectives, e.g., the width of the confidence interval of the link parameters. These optimization objectives can be cast as different optimal experimental design problems [Pukelsheim, 2006].

Below, we introduce two typical optimal experimental design objectives, A-Optimal and D-Optimal, and our model can handle other OED objectives. A-Optimal experimental design [Pukelsheim, 2006, López-Fidalgo, 2023] minimizes the trace of the inverse of the FIM $\mathbf{I}(\boldsymbol{\mu}; \boldsymbol{\phi})$ with respect to the allocation $\boldsymbol{\phi}$, i.e. $\text{tr}(\mathbf{I}^{-1}(\boldsymbol{\mu}; \boldsymbol{\phi}))$. This quantity is a lower bound for the average of the variances of the estimated link parameters $\sum_{\ell \in \mathcal{L}} \text{Var}(\hat{\mu}_\ell)$, when the estimator is unbiased. D-Optimal experimental design [López-Fidalgo, 2023] minimizes the reciprocal of the determinant of the FIM $\mathbf{I}(\boldsymbol{\mu}; \boldsymbol{\phi})$ with respect to the allocation $\boldsymbol{\phi}$, which minimizes the volume of the confidence ellipsoid of the estimated parameters.

In this paper, we denote $F(\boldsymbol{\mu}; \boldsymbol{\phi})$ as a general optimal experimental design criterion and denote $\boldsymbol{\phi}^*(\boldsymbol{\mu}) := \arg \min_{\boldsymbol{\phi}} F(\boldsymbol{\mu}; \boldsymbol{\phi})$ as the optimal allocation function given parameter $\boldsymbol{\mu}$ and OED criterion F .³ For example, in A-optimal scenario, we have $F(\boldsymbol{\mu}; \boldsymbol{\phi}) = \text{tr}(\mathbf{I}^{-1}(\boldsymbol{\mu}; \boldsymbol{\phi}))$, and in D-optimal scenario, we have $F(\boldsymbol{\mu}; \boldsymbol{\phi}) = (\det(\mathbf{I}(\boldsymbol{\mu}; \boldsymbol{\phi})))^{-1}$.

³We slightly abuse the $\boldsymbol{\phi}^*$ notation without the input $(\boldsymbol{\mu})$ to denote the optimal allocation based on the actual parameters.

Procedure 1 Online Experimental Design for Network Tomography

Input: \mathcal{M} (set of probes), \mathcal{N} (set of nodes), \mathcal{L} (set of links), T (number of decision rounds), F (optimal experimental design criterion)

1: **for** each time slot $t = 1, 2, \dots, T$ **do**

2: Select a probe m_t from set \mathcal{M} to perform the network tomography once

3: Observe $\mathbf{Y}_{m_t,t} = (Y_{n,t})_{n \in \mathcal{N}_{m_t}}$ from all destination nodes $n \in \mathcal{N}_{m_t,t}$ of the probe m_t

4: Update the parameters and estimates $\hat{\boldsymbol{\mu}}_t$

5: **end for**

Output: $\hat{\boldsymbol{\phi}}^*$ (estimated optimal allocation)

2.5 Online Experimental Design Problem and Objective Formulation

As the tomography task aims to reveal the values of the unknown network parameters $\boldsymbol{\mu}$, we formulate the tomography task as an online experimental design problem with a total of $T \in \mathbb{N}^+$ decision rounds. In each decision round $t \leq T$, the learner selects one tomography probe m_t and then observes the received signals $\mathbf{Y}_{m_t,t}$ in the destination nodes $n \in \mathcal{N}_{m_t}$ of this probe. The learner then updates the estimates of the network parameters based on the received signals until the end of the T decision rounds. Denote $S_{m,t}$ as the number of times that a specific algorithm performs probe m up to time slot t , and $\boldsymbol{\phi}_t = (S_{m,t}/t)_{m \in \mathcal{M}}$ as the actual allocation ratio of an algorithm at time step t . The online experimental design problem is summarized in Procedure 1.

As the goal of optimal experimental design (OED) is to minimize the function $F(\boldsymbol{\mu}; \boldsymbol{\phi})$ in terms of the allocation $\boldsymbol{\phi}$, we take the difference between $F(\boldsymbol{\mu}; \boldsymbol{\phi}_T)$ of the concerned algorithm and the minimum $F(\boldsymbol{\mu}; \boldsymbol{\phi}^*)$ with optimal allocation $\boldsymbol{\phi}^*$ as our objective, that is,

$$R_T := F(\boldsymbol{\mu}; \boldsymbol{\phi}_T) - F(\boldsymbol{\mu}; \boldsymbol{\phi}^*).$$

We follow the online learning literature and name the metric as *regret* since it describes the gap between the performed algorithm and the hindsight optimal.⁴ It is important to note that it differs from cumulative regret, which is the sum over all T rounds. The cumulative regret is unsuitable in our setting since $\boldsymbol{\phi}_T$ already considers all probes up to the end time T . Our regret measures an algorithm's convergence rate: The smaller the regret, the better the algorithm performs. For instance, in the A-Optimal design with unbiased estimators, a small regret implies a small MSE of the estimated parameters. Especially in linear regression, the difference divided by the number of rounds T , i.e., $(\text{tr } \mathbf{I}^{-1}(\boldsymbol{\mu}; \boldsymbol{\phi}_T) - \text{tr } \mathbf{I}^{-1}(\boldsymbol{\mu}; \boldsymbol{\phi}^*))/T$, equals the MSE of the parameter estimates [Fontaine et al., 2021].

⁴Some literature may refer to this regret definition as *simple regret*, the performance gap at the end of the online learning process, to differentiate from the cumulative regret.

3 OPAL: An Algorithm for Online Experimental Design

We propose an online experimental design algorithm with the aim to estimate link parameters μ and to approach the optimal allocation ϕ^* as close as possible. Given an OED criterion F and a network tomography model with parameters μ , as discussed in Section 2.4, there exists an optimal allocation $\phi^* = \arg \min_{\phi} F(\mu; \phi)$ which most accurately estimates the link parameters μ . However, without knowledge of link parameters μ a priori, it is challenging for an online algorithm to achieve the exactly optimal allocation ϕ^* during a finite number of rounds, T . This difficulty is due to the fact that the final allocation ratio ϕ_T is the accumulation of its whole probe sequence over all T decisions, and many of the early probe decisions, accounted for in the final ratio ϕ_T , are made without accurate estimates of the link parameters μ . Therefore, the actual allocation ϕ_T will inevitably deviate from ϕ^* .

We propose an online tomography algorithm that dynamically chases the estimated optimal probe allocation, called Online Probe Allocation (OPAL). The key idea of OPAL is inspired by the “chasing the (theoretical) optimal bound” idea used in multi-armed bandits literature, e.g., the optimal sampling algorithm that minimizes the regret of any structured bandits in Combes et al. [2017] and the Track-and-Stop algorithm achieving the optimal sample complexity for best arm identification in Garivier and Kaufmann [2016].

While we use the high-level idea of chasing from prior literature, the design of OPAL for the network tomography problem poses *several unique challenges* that make it impossible to directly apply existing algorithmic designs to our problem requiring a substantially different analysis than previous bandit algorithms [Combes et al., 2017, Garivier and Kaufmann, 2016]. The main difference is that the feedback mechanism in network tomography is more complex: one scalar observation (e.g., obtained by a unicast probe) can be non-linearly related to multiple link parameters along a path, and a vector observation (e.g., obtained by a multicast probe) may depend on even more link parameters through a set of non-linear relations. Indeed, this non-linearity is far more involved than the simple feedback mechanism in the bandit learning problems, where one scalar feedback usually corresponds precisely to one unknown parameter or a linear combination of unknown parameters, and independence across observations is often assumed. This non-linearity and correlation in the feedback mechanism of network tomography make the problem more challenging, requiring a different algorithmic design and analysis.

We first present the basic version of OPAL in Section 3.1 and then introduce a lazy update strategy in Section 3.2 to reduce the computational cost of the algorithm.

3.1 OPAL Algorithm Design

OPAL (presented in Algorithm 2) consists of two phases: (a) an initial sampling

Algorithm 2 Optimal Probe Allocation (OPAL)

Input: \mathcal{M} (set of probes), \mathcal{N} (set of nodes), \mathcal{L} (set of links), T (number of decision rounds), F (optimal experimental design criterion), MLE (estimator), $\mathbf{S}_0 := (S_{m,0})_{m \in \mathcal{M}}$ (initial sample sizes)

Initialize: $\mathcal{H}_0 \leftarrow \emptyset$ (history), $\hat{\boldsymbol{\mu}}_0 \leftarrow \mathbf{0}$ (parameter estimates), $T_0 \leftarrow \sum_{m \in \mathcal{M}} S_{m,0}$ (initial length)

```

1: for each time step  $t = 1, 2, \dots, T$  do
2:   if  $\exists m \in \mathcal{M} : S_{m,t} < S_{m,0}$  then                                 $\triangleright$  Initial sampling phase
3:      $m_t \leftarrow$  randomly pick from set  $\{m \in \mathcal{M} : S_{m,t} < S_{m,0}\}$ 
4:   else                                                                 $\triangleright$  Chasing phase
5:      $\hat{\boldsymbol{\mu}}_t \leftarrow \text{MLE}(\mathcal{H}_{t-1})$                                  $\triangleright$  Use MLE to update the parameter
       estimates  $\hat{\boldsymbol{\mu}}_t$ 
6:      $\hat{\phi}_t^* \leftarrow \arg \min_{\phi} F(\hat{\boldsymbol{\mu}}_t; \phi)$                              $\triangleright$  Calculate estimated optimal
       allocation
7:      $m_t \leftarrow \arg \max_{m \in \mathcal{M}} \hat{\phi}_{m,t}^* - (S_{m,t}/t)$                  $\triangleright$  Chase the estimated
       allocation
8:   end if
9:   Perform probe  $m_t$  and observe signals  $\mathbf{Y}_{m_t,t} = (Y_{n,t})_{n \in \mathcal{N}_{m_t}}$  for its desti-
       nation nodes
10:   $\mathcal{H}_t \leftarrow \mathcal{H}_{t-1} \cup \{(m_t, \mathbf{Y}_{m_t,t})\}$ ,  $S_{m_t,t} \leftarrow S_{m_t,t-1} + 1$  and  $S_{m,t} \leftarrow S_{m,t-1}$  for
       all  $m \neq m_t$ 
11: end for

```

Output: $\hat{\boldsymbol{\mu}}_{T+1} \leftarrow \text{MLE}(\mathcal{H}_T)$ (final estimates) and $\hat{\phi}_{T+1} \leftarrow \arg \max_{\phi} F(\hat{\boldsymbol{\mu}}_{T+1}; \phi)$ (final allocation)

Algorithm 3 Lazy Update for OPAL (replace OPAL’s Lines 5 and 6, called OPAL-lazy)

Input: inputs of OPAL and the integer B (batch size for lazy update)

```

1: if  $t \equiv 1 \pmod{B}$  then                                ▷ Lazy update
2:    $\hat{\boldsymbol{\mu}}_t \leftarrow \text{MLE}(\mathcal{H}_{t-1})$                 ▷ Use MLE to update the mean estimates  $\hat{\boldsymbol{\mu}}_t$ 
3:    $\hat{\boldsymbol{\phi}}_t^* \leftarrow \arg \min_{\boldsymbol{\phi}} F(\hat{\boldsymbol{\mu}}_{t-1}; \boldsymbol{\phi})$     ▷ Estimated optimal allocation
4: else
5:    $\hat{\boldsymbol{\phi}}_t^* \leftarrow \hat{\boldsymbol{\phi}}_{t-1}^*$                                 ▷ No update
6: end if
```

phase (Line 3) and (b) a chasing phase (Lines 5-7). The initial phase takes the initial sample sizes $\mathcal{S}_0 = (S_{m,0})_{m \in \mathcal{M}}$ as input and performs each probe $m \in \mathcal{M}$ accordingly (Lines 2-3). Collecting these $T_0 := \sum_{m \in \mathcal{M}} S_{m,0}$ initial samples ensures that the first estimates $\hat{\boldsymbol{\mu}}_{T_0}$ for link parameters at Line 5 are not too far away from the true parameters $\boldsymbol{\mu}$. The input initial samples \mathcal{S}_0 can either be set universally as fixed values for guaranteed good performance (discussed in Section 4.2) or determined by the specific network tomography task and prior knowledge of the network case by case (details discussed in two case studies in Sections 5.1 and 6.1).

The chasing phase proceeds step by step for each of the remaining time steps $t = T_0 + 1, T_0 + 2, \dots, T$. Denote $S_{m,t}$ as the number of times that the probe m is performed up to and including time t , and use vector $\mathbf{S}_t := (S_{m,t})_{m \in \mathcal{M}}$ to represent all the sample sizes. For each time step $t > T_0$, the algorithm first updates the MLE estimates $\hat{\boldsymbol{\mu}}_t$ of the network parameters using the latest history $\mathcal{H}_{t-1} = \{(m_s, \mathbf{Y}_{m_s,s})\}_{s=1}^{t-1}$ (Line 5). With the updated estimates $\hat{\boldsymbol{\mu}}_t$, the algorithm generates an *estimated optimal allocation* $\hat{\boldsymbol{\phi}}_t^*$ based on the latest link parameter estimates $\hat{\boldsymbol{\mu}}_t$ (Line 6). Then, the algorithm subtracts the actual allocation \mathbf{S}_t/t from the estimated optimal allocation $\hat{\boldsymbol{\phi}}_t^*$ element-wise (both are M -entry vectors), where the (possibly negative) entries of the output vector represent the inadequacy of the allocated fractions to each probe. Last, the algorithm performs the probe m_t with the worst (highest) allocation inadequacy once (Line 7)—*chasing the estimated optimal allocation* $\hat{\boldsymbol{\phi}}_t^*$ —to collect a new observation, and updates the sample sizes \mathbf{S}_t (Lines 9-10).

The above estimated optimal allocation chasing step is the core of OPAL, which dynamically adjusts the probe allocation based on the estimated optimal allocation $\hat{\boldsymbol{\phi}}_t^*$ at each time step t . After both phases, the algorithm outputs the final MLE estimates $\hat{\boldsymbol{\mu}}_{T+1}$ and final estimated optimal allocation $\hat{\boldsymbol{\phi}}_{T+1}^*$.

3.2 OPAL with lazy updates

Lines 5 and 6 in OPAL involve the MLE estimation and the estimated optimal allocation calculation, both of which can incur nontrivial computation costs. While one may derive analytical expressions for the MLE and optimal allocation for some specific network tomography models (as shown in our two case studies

in Sections 5.1 and 6.1), the general case may require computationally expensive numerical optimizations. To reduce the computation cost, we can replace Lines 5 and 6 in OPAL with the lazy update strategy in Algorithm 3 (denoted as OPAL-lazy). The OPAL-lazy algorithm updates the MLE estimates and the estimated optimal allocation every B time steps, and in the other time steps, it keeps the estimated optimal allocation unchanged. Varying the input batch size B can trade off the computation cost and the performance of OPAL.

4 Analysis

In this section, we analyze the performance of OPAL. We start with two critical conditions for the network tomography tasks (Section 4.1) and then present the main theorem that characterizes the regret of the algorithm (Section 4.2) based on these conditions.

4.1 Two Conditions on Network Tomography

We present two general conditions for the network tomography problem, which are crucial for the regret analysis of OPAL. Both conditions are natural and typically fulfilled in practice. Later in Sections 5.1 and 6.1, we verify both conditions in the classical and quantum network tomography case studies, respectively.

Condition 1 (Lipschitz Continuity). *The optimal experimental design criterion $F(\boldsymbol{\mu}; \boldsymbol{\phi})$ is Lipschitz continuous with respect to the allocation $\boldsymbol{\phi}$. That is, for some constant $\alpha > 0$ and any two allocations $\boldsymbol{\phi}, \boldsymbol{\phi}' \in \mathcal{F}$ where $\mathcal{F} \subseteq \Delta^{M-1}$ is the set of all feasible allocations that support the parameter identifiability,⁵ we have*

$$F(\boldsymbol{\mu}; \boldsymbol{\phi}) - F(\boldsymbol{\mu}; \boldsymbol{\phi}') \leq \alpha \|\boldsymbol{\phi} - \boldsymbol{\phi}'\|_{\infty}.$$

Further, the optimal allocation function $\boldsymbol{\phi}^(\boldsymbol{\mu})$ is Lipschitz continuous with respect to $\boldsymbol{\mu}$. That is, for some constant $\beta > 0$ and any two sets of feasible network parameters $\boldsymbol{\mu}, \boldsymbol{\mu}'$, we have*

$$\|\boldsymbol{\phi}^*(\boldsymbol{\mu}) - \boldsymbol{\phi}^*(\boldsymbol{\mu}')\|_{\infty} \leq \beta \|\boldsymbol{\mu} - \boldsymbol{\mu}'\|_{\infty}.$$

Lipschitz continuity is a common condition in practical scenarios, as it implies that the network tomography problem is well-behaved, and the optimal allocation $\boldsymbol{\phi}^*$ is stable with respect to the network parameters $\boldsymbol{\mu}$. For example, as long as function $F(\boldsymbol{\mu}; \boldsymbol{\phi})$ is a continuous function and differentiable in terms of $\boldsymbol{\phi}$ when $\boldsymbol{\phi} \in \Delta^{M-1}$, it is Lipschitz continuous in any compact subset of Δ^{M-1} [O’Searcoid, 2006, Theorem 9.5.1].

⁵The set \mathcal{F} contains all interior points and perhaps a part of the boundary points of the simplex set Δ^{M-1} . For example, in the classical loss star network tomography via unicasts in Section 5.1, all unicast probes are necessary for identifying the network parameters. Hence, any allocation on the boundary (i.e., allocations contain zero entries) does not correspond to a feasible allocation, and $\mathcal{F} = \Delta^{M-1} \setminus \partial\Delta^{M-1}$.

Condition 2 (Estimator Concentration / Confidence Interval). *At any decision round t , the confidence interval (with confidence $1 - \delta$ for parameter $\delta \in (0, 1)$) for any parameter μ_ℓ of a link $\ell \in \mathcal{L}$ is an interval centered at its MLE estimate $\hat{\mu}_{\ell,t}$ with radius $\sum_{m \in \mathcal{M}} c_{\ell,m} (\log \delta^{-1} / S_{m,t})^{\gamma_{\ell,m}}$, where $c_{\ell,m} \geq 0, \gamma_{\ell,m} > 0$ are parameters depending on the network and tomography probes, and $S_{m,t}$ is the number of times that probe m is performed up to round t .*

Condition 2 describes the concentration rate of the MLE estimator (or any other estimator) in terms of the sample times $S_{m,t}$ of all probes m . This is a finite-time (non-asymptotic) statement. With the central limit theorem, one can derive an asymptotic version of the confidence interval with radius $z_{\delta/2} \sqrt{I_{\ell,\ell}^{-1}(\boldsymbol{\mu}; \boldsymbol{\phi}_{\text{asym}}) / S_{m,t}}$ [Cáceres et al., 1999, Theorem 4], where $z_{\delta/2}$ is the $\delta/2$ quantile of the standard normal distribution and $I_{\ell,\ell}^{-1}(\boldsymbol{\mu}; \boldsymbol{\phi}_{\text{asym}})$ is the (ℓ, ℓ) -entry of the inverse of the Fisher information matrix with the asymptotical allocation $\boldsymbol{\phi}_{\text{asym}}$. This implies that the concentration rate $\gamma_{\ell,m}$ of the probing experimental m for the parameter of link ℓ approaches $1/2$ for large sample sizes.

4.2 Regret (Convergence Rate) Analysis of OPAL

In this section, we present the main theorem that characterizes the regret of OPAL. We recall the probe allocation ratio of the algorithm at time t as $\phi_t := (S_{m,t}/t)_{m \in \mathcal{M}}$.

Theorem 1. *Given Conditions 1 and 2 with $\delta = 1/(LT^2)$, for time horizon $T > 0$, initial probe times $S_{m,0} = \xi T$, $m \in \mathcal{M}$, for any $\xi \in (0, 1)$, with probability of at least $1 - 1/T$, OPAL satisfies,*

$$R_T = F(\boldsymbol{\mu}; \phi_T) - F(\boldsymbol{\mu}; \phi^*) \leq C \left(\frac{\log(LT)}{\xi T} \right)^{\gamma_{\min}} + \alpha \xi \mathbb{1} \left\{ \exists m \in \mathcal{M} : \phi_m^* < \xi + C \left(\frac{\log(LT)}{\xi T} \right)^{\gamma_{\min}} \right\}, \quad (1)$$

where $C = O(\alpha \beta c_{\max})$ is a constant that depends on the probing experiments and network, independent of time horizon T , α and β are from Condition 1, parameters $c_{\max} := \max_{\ell \in \mathcal{L}} \sum_{m \in \mathcal{M}} c_{\ell,m}$ and $\gamma_{\min} := \min_{(\ell,m) \in \mathcal{L} \times \mathcal{M} : \gamma_{\ell,m} > 0} \gamma_{\ell,m}$ are from Condition 2, and $\mathbb{1}\{\cdot\}$ is the indicator function.

Implications of Theorem 1. Theorem 1 characterizes the regret of OPAL. To better understand the regret, we discuss several special cases. *First*, for many network tomography tasks, even without knowing the actual network parameters, one can select a compact set of probing experiments \mathcal{M} such that each probe in the set is needed at least a certain threshold ratio—that is, $\phi_m^* > \phi_{\text{threshold}}$ for all probes $m \in \mathcal{M}$ —to identify the network parameters. One can set ξ in Theorem 1 to this threshold, and then the second term in the RHS of (1) vanishes, leading to a $\tilde{O}(T^{-\gamma_{\min}})$ regret. For example, in the case study in Section 5.1, spreading the first $O(\log T)$ time steps uniformly across each probe yields a rough estimate of the network parameters. With these estimates,

one can find such a threshold ratio and set ξ as the threshold to cancel the second term.

Second, one can always set $\xi = T^{-\frac{\gamma_{\min}}{1+\gamma_{\min}}}$ in Theorem 1, guaranteeing a decent $\tilde{O}(T^{-\frac{\gamma_{\min}}{1+\gamma_{\min}}})$ regret, independent of whether the second term of the regret in (1) can be canceled or not. For example, the second term cannot be canceled by any constant $\xi > 0$ in a scenario that the optimal allocation ϕ^* contains some zero entries, i.e., $\phi_m^* = 0$ for some probe m (e.g., the case study in Section 6.1). That is, when there are unavoidable inferior probes, letting $\xi = T^{-\frac{\gamma_{\min}}{1+\gamma_{\min}}}$ is a plausible choice, and OPAL yields a $\tilde{O}(T^{-\frac{\gamma_{\min}}{1+\gamma_{\min}}})$ regret, slightly worse than the $-\gamma_{\min}$ rate.

Third, from an asymptotic perspective (for large sample sizes) and by the central limit theorem, the concentration rate of Condition 2 would be $\gamma_{\ell,m} = 1/2$ for all probes m and links ℓ . Assuming the second term in (1) is canceled, the regret of OPAL becomes $\tilde{O}(T^{-\frac{1}{2}})$. This rate is near-optimal in the sense that, even for the online linear regression (simpler than our network tomography task), minimizing the regret for A-optimal design criterion (with the number of probes greater than that of links, $M > L$) is known to suffer at least a $\Omega(T^{-1/2})$ regret [Fontaine et al., 2021, Theorem 4].

4.2.1 Proof of Theorem 1

Overview. OPAL utilizes the actual allocation $\phi_t = (S_{m,t}/t)_{m \in \mathcal{M}}$ to “chase” the optimal allocation ϕ^* (Line 7). To show the convergence of the algorithm, we need to analyze the effectiveness of such a chasing strategy. That is, *how good is the actual allocation ϕ_t in approximating the optimal allocation ϕ^* as the algorithm proceeds?* Such an analysis is challenging due to the sequential decision-making nature of the process: On one hand, as the actual network parameters μ are unknown, the algorithm does not know the optimal allocation ϕ^* and, hence, needs to calculate the *estimated* optimal allocation $\hat{\phi}_t^*$ based on the parameter estimates $\hat{\mu}_t$. This introduces an *accuracy gap* in the chasing process. On the other hand, the actual allocation ϕ_t depends on all past probe decisions, which often lag behind the *time-varying* estimated optimal allocation $\hat{\phi}_t^*$. This introduces a *lag gap*. The proof of Theorem 1 bounds these two gaps.

Detailed proof of Theorem 1. After the initial sampling phase, we have $S_{m,t} = \xi T$ and $t = T_0 = M\xi T$. In addition, the gap between the estimated optimal allocation $\hat{\phi}_{T_0}^*$ and the actual optimal allocation ϕ^* can be characterized as follows.

$$\left\| \hat{\phi}_{T_0}^* - \phi^* \right\|_{\infty} \stackrel{(a)}{\leq} \beta \left\| \hat{\mu}_{T_0} - \mu \right\|_{\infty} \stackrel{(b)}{\leq} \beta \max_{\ell \in \mathcal{L}} \sum_{m \in \mathcal{M}} c_{\ell,m} \left(\frac{\log \delta}{\xi T} \right)^{\gamma_{\ell,m}} \stackrel{(c)}{\leq} \beta c_{\max} \left(\frac{\log \delta}{\xi T} \right)^{\gamma_{\min}}, \quad (2)$$

where inequality (a) is due to the second Lipschitz continuity in Condition 1, inequality (b) follows from the confidence radius of estimates in Condition 2 with a probability of at least $1 - L\delta$, and inequality (c) follows from the definition of $c_{\max} = \max_{\ell \in \mathcal{L}} \sum_{m \in \mathcal{M}} c_{\ell,m}$ and $\gamma_{\min} = \min_{(\ell,m) \in \mathcal{L} \times \mathcal{M}: \gamma_{\ell,m} > 0} \gamma_{\ell,m}$.

Next, we bound the regret — the difference between the OED criterion F of the actual allocation ϕ_T and the optimal allocation ϕ^* — as follows.

$$\begin{aligned}
F(\mu; \phi_T) - F(\mu; \phi^*) &\stackrel{(d)}{\leq} \alpha \|\phi_T - \phi^*\|_\infty \stackrel{(e)}{\leq} \alpha \|\phi_T - \hat{\phi}_T^*\|_\infty + \alpha \|\hat{\phi}_T^* - \phi^*\|_\infty \\
&\stackrel{(f)}{\leq} \alpha \|\phi_T - \hat{\phi}_T^*\|_\infty + \alpha \beta \|\hat{\mu}_T - \mu\|_\infty \stackrel{(g)}{\leq} \alpha \|\phi_T - \hat{\phi}_T^*\|_\infty + \alpha \beta \max_{\ell \in \mathcal{L}} \sum_{m \in \mathcal{M}} c_{\ell, m} (2 \log T / S_{m, T})^{\gamma_{\ell, m}} \\
&\stackrel{(h)}{\leq} \alpha \|\phi_T - \hat{\phi}_T^*\|_\infty + \alpha \beta c_{\max} \left(\frac{\log \delta}{\xi T} \right)^{\gamma_{\min}} \stackrel{(i)}{\leq} \alpha \left(\frac{1}{(1 - \xi)T} + 3\beta c_{\max} \left(\frac{\log \delta}{\xi T} \right)^{\gamma_{\min}} \right) + \alpha \beta c_{\max} \left(\frac{\log \delta}{\xi T} \right)^{\gamma_{\min}} \\
&= 4\alpha \beta c_{\max} \left(\frac{\log \delta}{\xi T} \right)^{\gamma_{\min}} + \frac{\alpha}{(1 - \xi)T},
\end{aligned}$$

where inequality (d) follows from the Lipschitz continuity of function F with respect to allocations ϕ in Condition 1, inequality (e) follows from the triangle inequality, inequality (f) follows from the Lipschitz continuity of the optimal allocation in function $\phi^*(\mu)$ concerning the network parameters μ in Condition 1, inequality (g) follows from the confidence radius of estimates in Condition 2, holding with a probability of at least $1 - L\delta$, inequality (h) is by telescoping the maximization term $\max_{\ell \in \mathcal{L}}$ and the sum $\sum_{m' \in \mathcal{M}}$ by their upper bounds, and $S_{m, T} \geq \xi T$ for any probing experimental m due to the initial sample phase input $\mathcal{S}_0 = (\xi T)_{m \in \mathcal{M}}$. Finally, inequality (i) is by (3) for deriving the first term in (1); the second term in (1) is derived by (4) (see below for a detailed derivation).

Last, we present the detailed telescoping derivation of inequality (i) in the above proof for bounding $\|\phi_T - \hat{\phi}_T^*\|_\infty$. The high-level derivation technique is illustrated in Fig. 3. We consider two cases: (1) all probes have optimal allocations greater than ξ , and (2) there exists at least one probe with optimal allocation less than ξ .

Case (1). When $\phi_m^* > \xi$ for all probes m , we have

$$\begin{aligned}
\|\phi_T - \hat{\phi}_T^*\|_\infty &\stackrel{(j)}{\leq} \|\phi_T - \hat{\phi}_{T_0}^*\|_\infty + \|\hat{\phi}_{T_0}^* - \hat{\phi}_T^*\|_\infty \\
&\stackrel{(k)}{\leq} \frac{1}{(1 - \xi)T} + \beta c_{\max} \left(\frac{\log \delta}{\xi T} \right)^{\gamma_{\min}} + \|\hat{\phi}_{T_0}^* - \hat{\phi}_T^*\|_\infty \quad (3) \\
&\stackrel{(l)}{\leq} \frac{1}{(1 - \xi)T} + 3\beta c_{\max} \left(\frac{\log \delta}{\xi T} \right)^{\gamma_{\min}},
\end{aligned}$$

where inequality (j) follows from the triangle inequality, inequality (k) is by noticing that while the chased estimated optimal allocation $\hat{\phi}_t^*$ changes over time, it always lies in the confidence interval of the initial estimated optimal allocation $\hat{\phi}_{T_0}^*$ in (2), and inequality (l) follows from applying triangle inequality to show that $\|\hat{\phi}_{T_0}^* - \hat{\phi}_T^*\|_\infty \leq \|\hat{\phi}_{T_0}^* - \phi^*\|_\infty + \|\phi^* - \hat{\phi}_T^*\|_\infty$, and both terms in RHS are less than $\beta c_{\max} \left(\frac{\log \delta}{\xi T} \right)^{\gamma_{\min}}$ as (2) shows.

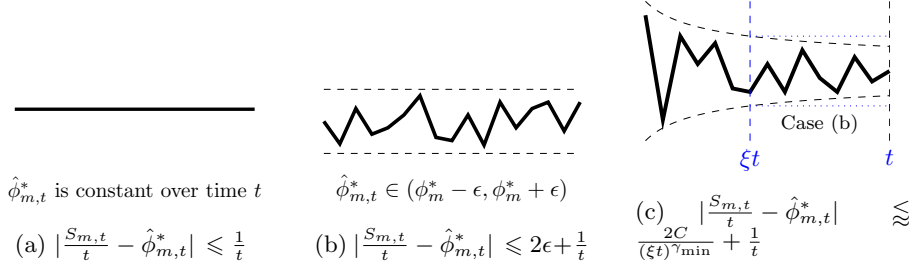


Figure 3: A high-level illustration of the novel bounding technique used in (3). The thick solid line is the chased allocation $\hat{\phi}_{m,t}^*$ varying over time, and the dashed black line is the confidence interval of the ground truth allocation ϕ_m^* . The derivation of (3) comes from two simplifications of the chasing step of Line 7 of Algorithm 2 in Figs. 3a and 3b. Fig. 3a: if the chased estimated optimal allocation $\hat{\phi}_t^*$ is fixed over time t , then the actual allocation ϕ_t is close to the chased allocation up to a distance of $1/t$; Fig. 3b: if the chased allocation $\hat{\phi}_t^*$ is changing over time t but its variation is bounded by an interval with width 2ϵ , then the empirical allocation is close to the final chased allocation up to $2\epsilon + 1/t$. The combination of these two simplifications leads to the bound in (3), illustrated in Fig. 3c.

Case (2). When there exists at least one probe m such that $\phi_m^* \leq \xi < \xi + \beta c_{\max} \left(\frac{\log \delta}{\xi T} \right)^{\gamma_{\min}}$, by modifying the derivation of inequality (3) and noticing that its LHS is for infinity norm, we have

$$\begin{aligned}
 \|\phi_T - \hat{\phi}_T^*\|_{\infty} &\leq \max_{m: \phi_m^* > \xi} \left| \phi_{m,T} - \hat{\phi}_{m,T}^* \right| + \max_{m: \phi_m^* \leq \xi + \beta c_{\max} \left(\frac{\log \delta}{\xi T} \right)^{\gamma_{\min}}} \left| \phi_{m,T} - \hat{\phi}_{m,T}^* \right| \\
 &\leq \frac{1}{(1 - \xi)T} + 7\beta c_{\max} \left(\frac{\log \delta}{\xi T} \right)^{\gamma_{\min}} + 2\xi,
 \end{aligned} \tag{4}$$

where the first maximization term follows the same derivation as (3) in Case (1), and the second term is by noticing that $\hat{\phi}_{m,t}^* \in \left(\phi_m^* - \beta c_{\max} \left(\frac{\log \delta}{\xi T} \right)^{\gamma_{\min}}, \phi_m^* + \beta c_{\max} \left(\frac{\log \delta}{\xi T} \right)^{\gamma_{\min}} \right)$ for all time slots t in the chasing phase with high probability, and hence the actual allocation ϕ_t , chasing the estimated optimal allocation $\hat{\phi}_t^*$, is also less than $\phi_m^* + \beta c_{\max} \left(\frac{\log \delta}{\xi T} \right)^{\gamma_{\min}}$. Therefore, the second term in (4) is at most $2 \left(\phi_m^* + \beta c_{\max} \left(\frac{\log \delta}{\xi T} \right)^{\gamma_{\min}} \right) \leq 2\xi + 4\beta c_{\max} \left(\frac{\log \delta}{\xi T} \right)^{\gamma_{\min}}$.

At the end, replacing δ by $1/(LT^2)$ yields the final regret bound. Over the proof procedure, the confidence interval in Condition 2 is applied multiple times. Applying a union bound of all these confidence interval applications leads to a failure probability of at most $LT\delta$, which becomes $1/T$ after the substitution. \square

5 Case Study for Classical Network Tomography

This section presents a case study on classical network tomography. In Section 5.1, we investigate loss tomography in a star network and verify the Lipschitz continuity of the A-optimal design and the concentration rate of the MLE estimator for the corresponding link parameters. We then provide empirical results in Section 5.2 for both star and general networks with comparisons against alternative baselines.

5.1 Analytical Case 1: Classical Star Network Unicast Setting

In this analytical case study, we examine loss tomography in a star network with L links, and we focus solely on unicast probes due to their analytical traceability. An example with 3 links is shown in Figure 1b. For the L -link star network, we select a set of $M = L$ probes that ensure identifiability of the link parameters $\boldsymbol{\mu}$. These M probes are represented by an $M \times L$ matrix $\mathbf{Q} \in \{0, 1\}^{M \times L}$, known as the *measurement matrix*, where $Q_{m,\ell} = 1$ if the m -th unicast probe passes through the ℓ -th link, and $Q_{m,\ell} = 0$ otherwise. In other words, each row of \mathbf{Q} corresponds to a probing experiment, with the two non-zero entries in each row indicating the source and destination of the unicast probe. Denote $\nu_m := \mu_{\ell_{m,1}}\mu_{\ell_{m,2}}$ as the success probability of the m -th probe, where $\ell_{m,1}$ and $\ell_{m,2}$ represent the source and destination nodes/links of the m -th probe, respectively. With measurement matrix \mathbf{Q} , we have $\log \boldsymbol{\nu} = \mathbf{Q} \log \boldsymbol{\mu}$.⁶

Lipschitz Continuity of the A-optimal Design

We select the A-optimal experimental design as the objective to verify the Lipschitz continuity in Condition 1. Based on the derivation in He et al. [2015, Theorem 6], we compute the trace of the inverse of the Fisher information matrix $\mathbf{I}(\boldsymbol{\mu}; \boldsymbol{\phi})$ for the L -link star network as follows,

$$F(\boldsymbol{\mu}; \boldsymbol{\phi}) = \text{tr } \mathbf{I}^{-1}(\boldsymbol{\mu}; \boldsymbol{\phi}) = \sum_{m=1}^M \frac{1}{\phi_m} A_m(\boldsymbol{\mu}), \quad (5)$$

where $A_m(\boldsymbol{\mu}) := \frac{1-\nu_m}{\nu_m} \sum_{\ell=1}^L \mu_\ell^2 \kappa_{\ell,m}$ is a function of the link parameters $\boldsymbol{\mu}$, and $\kappa_{\ell,m} := (\mathbf{Q}^{-1})_{\ell,m}$ denotes the (ℓ, m) -entry of the inverse of the measurement matrix \mathbf{Q} .

By the method of Lagrange multipliers, the A-optimal solution for minimizing $F(\boldsymbol{\mu}; \boldsymbol{\phi})$ is

$$\phi_m^* = \frac{\sqrt{A_m(\boldsymbol{\mu})}}{\sum_{m' \in \mathcal{M}} \sqrt{A_{m'}(\boldsymbol{\mu})}}, \quad \forall m \in \mathcal{M}. \quad (6)$$

⁶The log denotes the element-wise natural logarithm.

As the analytical solutions of the A-optimal design in (5) and (6) only contain basic calculations and are thus differentiable (recall $\mu_\ell \in (0, 1)$), we verify the Lipschitz continuity in Condition 1.

MLE Estimator for Link Parameters

Next, we present the MLE estimator for the link parameters $\boldsymbol{\mu}$. The MLE for the success probability of each probe ν_m is $\hat{\nu}_m = \frac{B_m}{S_m}$, where S_m is the number of times the m -th probe is performed, and B_m is the number of successful receptions among the S_m probes. The link parameters $\boldsymbol{\mu}$ can be expressed as a function of the success probabilities $\boldsymbol{\nu}$ in the form of $\log \boldsymbol{\mu} = (\mathbf{Q}^T \mathbf{Q})^{-1} \mathbf{Q}^T \log \boldsymbol{\nu}$. Using the invariance property of MLE under one-to-one transformations, the MLE estimator for the link parameters $\boldsymbol{\mu}$ is derived as

$$\hat{\boldsymbol{\mu}} = \exp((\mathbf{Q}^T \mathbf{Q})^{-1} \mathbf{Q}^T \log \hat{\boldsymbol{\nu}}) \stackrel{(a)}{=} \exp(\mathbf{Q}^{-1} \log \hat{\boldsymbol{\nu}}), \quad (7)$$

where equality (a) is a consequence of matrix \mathbf{Q} being square and invertible. This matrix form in (7) can be further expressed in an element-wise form as $\hat{\mu}_\ell = \prod_{m \in \mathcal{M}} \hat{\nu}_m^{\kappa_{\ell,m}}$ for every link $\ell \in \mathcal{L}$.

Concentration Rate of the MLE Estimator

Next, we turn to examine the confidence interval (concentration rate) in Condition 2 for the MLE estimator in (7). The next two lemmas, proven in Appendix A, show the impact of the entries of the inverse matrix \mathbf{Q}^{-1} on the MLE estimator for the link parameters $\boldsymbol{\mu}$.

Lemma 2. *For any estimator $\hat{\mu}_\ell = \prod_{m \in \mathcal{M}} \hat{\nu}_m^{\kappa_{\ell,m}}$, where the $\kappa_{\ell,m} \in \mathbb{R}$ is the ℓ^{th} -row, m^{th} -column entry of matrix \mathbf{Q}^{-1} and defining $\kappa'_{\ell,m} := \min\{\frac{1}{2}, |\kappa_{\ell,m}|\}$, we have, with a probability of at least $1 - \delta$,*

$$\mu_\ell \in \left(\hat{\mu}_\ell - \sum_{m \in \mathcal{M}: \kappa_{\ell,m} \neq 0} c_{m,\ell} \left(\frac{\log(\delta^{-1}/M)}{S_m} \right)^{\kappa'_{\ell,m}}, \hat{\mu}_\ell + \sum_{m \in \mathcal{M}: \kappa_{\ell,m} \neq 0} c_{m,\ell} \left(\frac{\log(\delta^{-1}/M)}{S_m} \right)^{\kappa'_{\ell,m}} \right),$$

where $c_{m,\ell}$'s are positive constants depending only on the network topology and link parameters.

As Lemma 2 shows, the actual concentration rate (exponents $\kappa'_{\ell,m}$) of the MLE depends on the entries of the inverse measurement matrix \mathbf{Q}^{-1} . For unicast loss tomography in the star network, we prove a lemma that characterizes the inverse matrix \mathbf{Q}^{-1} as follows,

Lemma 3. *For unicast loss tomography in a star network, inverse measurement matrix \mathbf{Q}^{-1} only has $\{0, \pm \frac{1}{2}, \pm 1\}$ entries.*

Combining both lemmas yields the concentration rate of the MLE estimator for the link parameters $\boldsymbol{\mu}$ in the star network as follows,

Theorem 4. *For unicast star network we have, with a probability of at least $1 - \delta$,*

$$\mu_\ell \in \left(\hat{\mu}_\ell - \sum_{m \in \mathcal{M}: \kappa_{\ell,m} \neq 0} c_{m,\ell} \sqrt{\frac{\log(\delta^{-1}/M)}{S_m}}, \hat{\mu}_\ell + \sum_{m \in \mathcal{M}: \kappa_{\ell,m} \neq 0} c_{m,\ell} \sqrt{\frac{\log(\delta^{-1}/M)}{S_m}} \right). \quad (8)$$

This verifies Condition 2 regarding the concentration rate of the MLE estimator for the link parameters in the unicast star network. Specifically, the exponent parameters are $\gamma_{m,\ell} \in \{0, \frac{1}{2}\}$, resulting in a minimum nonzero exponent $\gamma_{\min} = \frac{1}{2}$.

Regret of OPAL on the Classical Star Network

With the confidence interval in (8) and $\delta = 1/LT^2$, we know that $O(\log T)$ samples for each unicast probe suffice to estimate the link parameters μ with relatively good accuracy. Furthermore, utilizing the Lipschitz continuity of the A-optimal design allocation in (6), one can derive a lower bound ξ for the optimal allocation ratio ϕ_m^* for all probes $m \in \mathcal{M}$. By using this constant lower bound ξ as input to Theorem 1, the second term of the general regret bound in (1) is canceled. Consequently, the regret of OPAL for the A-optimal design under the loss star network is expressed as

$$R_T = \text{tr } \mathbf{I}^{-1}(\mu; \phi_T) - \text{tr } \mathbf{I}^{-1}(\mu; \phi^*) = O\left(\left(\frac{\log T}{T}\right)^{\frac{1}{2}}\right).$$

The feedback space for multicast probes is significantly larger than that for unicast, making it challenging to directly verify the Lipschitz continuity and the concentration condition of the MLE estimator. Other indirect methods, such as numerically plotting their curves, may be able to verify both conditions; we leave this for future work.

5.2 Simulations for Classical Network Tomography

In this section, we present numerical simulations to evaluate the performance of the proposed online probe allocation (OPAL) algorithm in terms of A-optimal experimental design for loss tomography in classical networks under unicast (beyond star network in the above analytical case study). We consider three baselines: an iterative algorithm proposed in [He et al., 2015, Algorithm 2], the A-Optimal allocation, and a uniform allocation. The iterative algorithm is batch-based. It performs probes in each batch (consisting of 100 time steps) according to its iteratively updated allocation. The initial sampling phase of OPAL is set to $T_0 = 0.05 \cdot T$ uniformly over all probes. The A-optimal allocation policy follows the ϕ^* that minimize the A-optimal experimental design $F(\mu, \phi)$ assuming the prior knowledge of link parameters μ , and the uniform allocation policy follows the $\phi_{\text{unif.}} = \mathbf{1}/L$. All experiments are conducted for five scenarios,

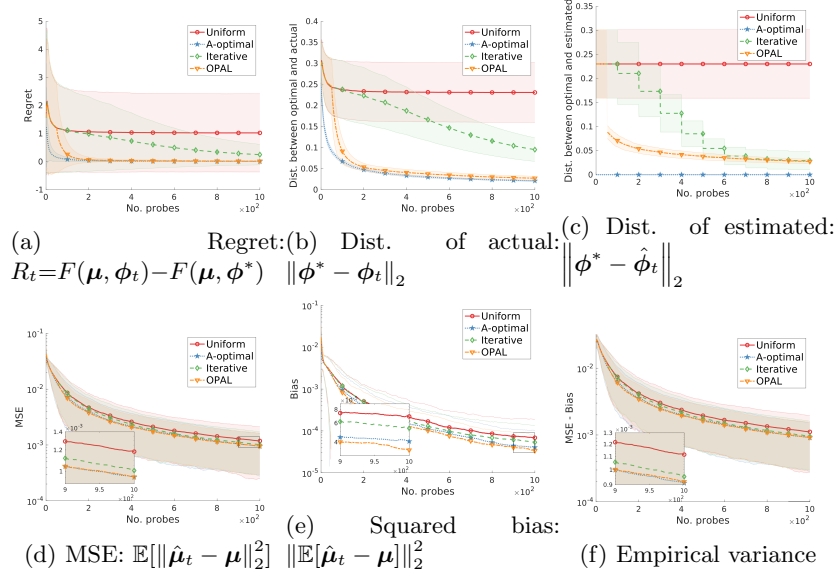


Figure 4: Comparison of algorithms for 3-link star networks

each of which uses randomly picked link parameters μ_ℓ . For each scenario, we conduct 100 Monte Carlo simulations and take their average as the performance under that scenario. In the final figures, the solid lines represent the average of these scenarios, and the shaded areas represent their standard deviation across the 100-run average for each scenario.

We conducted three experiments. The first two compare the performance of OPAL with other baselines: a 3-link star network, as shown in Figure 4, and a random Erdős-Rényi (ER) network with 10 nodes and approximately 30 links (the specific number varies across different scenarios), illustrated in Figure 5. The third experiment investigates the impact of lazy update batch sizes B on OPAL-lazy (Algorithm 3) applied to in the ER network, and its detail figures are deferred to Appendix B.

For each of these three experiments, we present six subfigures: (a) regret, (b) the distance between the actual allocation and the optimal allocation, (c) the distance between the estimated allocation and the optimal allocation, (d) the mean squared error (MSE), (e) the squared bias of the estimated loss rates, and (f) the empirical variance, which is equal to the MSE minus the squared bias. *Smaller values for these six metrics indicate better algorithm performance.* Regret (subfigure (a)) is the primary objective that OPAL seeks to minimize. The key difference between metrics (b) and (c) is that (b) evaluates the actual allocation ϕ_t chosen by the algorithm, while (c) assesses the latest estimated allocation $\hat{\phi}_t$.

Figures 4 and 5 highlight the following key findings: (I) OPAL consistently outperforms both the iterative algorithm and uniform allocation across all met-

rics. Additionally, OPAL often matches the performance of the A-optimal allocation (offline optimal). (II) The trends in regret ($F(\boldsymbol{\mu}, \boldsymbol{\phi}_t) - F(\boldsymbol{\mu}, \boldsymbol{\phi}^*)$) in subfigures (a) closely follow the trends in the distance between the actual allocation and the optimal allocation $\|\boldsymbol{\phi}_t - \boldsymbol{\phi}^*\|_2$ in subfigures (b). This aligns with the identified Lipschitz continuity of the A-optimal design criterion (Condition 1). (III) Comparing the distance between the estimated allocation and the optimal allocation $\|\boldsymbol{\phi}^* - \hat{\boldsymbol{\phi}}_t\|_2$ in subfigures (c) with the distance of the actual allocation in subfigures (b), we observe that while both OPAL and the iterative algorithm produce good estimated allocations $\hat{\boldsymbol{\phi}}_t$ after a sufficient number of probes in subfigures (c), only OPAL achieves a good actual allocation $\boldsymbol{\phi}_t$ close to the optimal in subfigures (b). This underscores the importance of OPAL’s online nature, particularly the chase optimal bound strategy, in achieving a favorable actual allocation and minimizing regret.

(IV) Although the A-optimal experimental design aims to minimize the total variance of the estimated parameters (which minimizes the MSE if the estimator is unbiased), the trends of the MSE in subfigures (d) deviate from those of regret in subfigures (a). This deviation arises because the MLE estimator in loss tomography is biased, as evident in the bias subfigures (e), thereby breaking the equivalence between MSE and $\text{Var}(\boldsymbol{\mu})$ minimized by the A-optimal design. Lastly, (V) to further evaluate algorithm performance concerning the biased Cramér-Rao bound (distinct from the A-optimal metric $F(\boldsymbol{\mu}, \boldsymbol{\phi})$ in subfigures (a)), we plot the empirical estimates of the variances in subfigures (f), i.e., MSE minus squared bias, $\mathbb{E}[\|\hat{\boldsymbol{\mu}}_t - \boldsymbol{\mu}\|_2^2] - \|\mathbb{E}[\hat{\boldsymbol{\mu}}_t - \boldsymbol{\mu}]\|_2^2$, which is lower bounded by the biased Cramér-Rao bound (detailed in Appendix C). The results demonstrate that OPAL’s variance performance surpasses the two baselines and closely approaches that of the A-optimal allocation. This indicates that OPAL achieves better performance even under the consideration of the biased Cramér-Rao bound.

6 Case Study for Quantum Network Tomography

This section presents a case study on the bit-flip quantum channel tomography in the quantum star network. Section 6.1 verifies the conditions outlined in Section 4.1 and presents the specific regret of OPAL. Subsequently, in Section 6.2, we provide empirical results for the quantum scenario, validating the superiority of OPAL over existing methods.

6.1 Analytical Case 2: Quantum Bit-Flip Star Network Multicast Setting

We consider a L -link star network for A-optimal experimental design, where each link $\ell \in \mathcal{L}$ is a *quantum* bit-flip channel with an unknown bit-flip probability μ_ℓ . As no unicast protocol in quantum network tomography was proposed, we

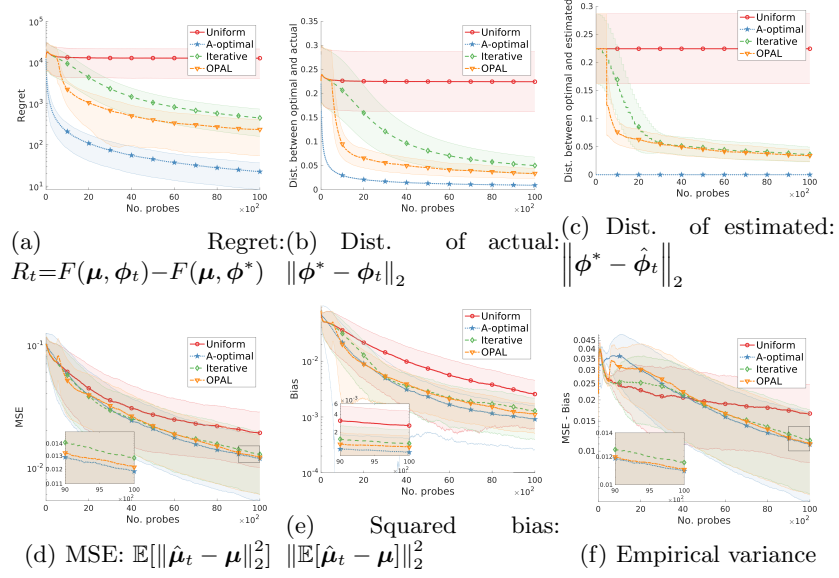


Figure 5: Comparison of algorithms for ER networks

consider the root-independent (RI) multicast protocol devised by [De Andrade et al. \[2023\]](#). The probing experiment set \mathcal{M} consists of $M = L$ multicast probes, each selecting one link $\ell \in \mathcal{L}$ as the root, multicasting quantum states to the remaining $L - 1$ links, and measuring the received qubits at these links. Denote $A_{m,\ell}$ as the total non-flip counts from the measurements of probe m for each link $\ell \neq m$. Further details regarding the bit-flip channel and the RI multicast protocol are provided in Section 2.3 and Figure 2.

Lipschitz Continuity of the A-Optimal Design

We first derive the trace of the inverse of the Fisher information matrix for the quantum star network with bit-flip quantum channels as follows,

$$F(\mu; \phi) = \text{tr } I^{-1}(\mu; \phi) = \sum_{m \in \mathcal{M}} \frac{(1 - \mu_m)\mu_m}{1 - \phi_m}.$$

This expression verifies the Lipschitz continuity of the A-optimal design criterion (first part of Condition 1). Next, by applying the method of Lagrange multipliers, we derive the A-optimal solution ϕ^* for the quantum star network with bit-flip quantum channels. The optimal allocation depends on the link parameters, as presented in (9) of Algorithm 4. Specifically, one first sorts the links by the value of $\sqrt{(1 - \mu_\ell)\mu_\ell}$ in descending order, and then iteratively eliminates the link with the largest value of $\sqrt{(1 - \mu_\ell)\mu_\ell}$ until the condition in Line 1 is not satisfied. The optimal allocation is then given by (9) for the remaining links in the candidate set \mathcal{M}_{opt} .

Algorithm 4 A-Optimal Allocation for Bit-Flip Tomograph in Quantum Star Networks

Input: link parameters μ and candidate probe set $\mathcal{M}_{\text{opt}} \leftarrow \{1, 2, 3, \dots, M\}$
 $(M = L)$

1: **while** $\sum_{\ell \in \mathcal{M}_{\text{opt}}} \sqrt{(1 - \mu_{\ell})\mu_{\ell}} - (|\mathcal{M}_{\text{opt}}| - 1) \max_{\ell' \in \mathcal{M}_{\text{opt}}} \sqrt{(1 - \mu_{\ell'})\mu_{\ell'}} < 0$
do
2: $\mathcal{M}_{\text{opt}} \leftarrow \mathcal{M}_{\text{opt}} \setminus \{\arg \max_{\ell' \in \mathcal{M}_{\text{opt}}} \sqrt{(1 - \mu_{\ell'})\mu_{\ell'}}\}$
3: **end while**

Output:
$$\phi_{\ell}^* = \begin{cases} \frac{\sum_{\ell' \in \mathcal{M}_{\text{opt}}} \sqrt{(1 - \mu_{\ell'})\mu_{\ell'}} - (|\mathcal{M}_{\text{opt}}| - 1) \sqrt{(1 - \mu_{\ell})\mu_{\ell}}}{\sum_{\ell' \in \mathcal{M}_{\text{opt}}} \sqrt{(1 - \mu_{\ell'})\mu_{\ell'}}} & \text{for } \ell \in \mathcal{M}_{\text{opt}}, \\ 0 & \text{for } \ell \notin \mathcal{M}_{\text{opt}}. \end{cases} \quad (9)$$

While the expression for the optimal allocation solution ϕ^* in (9) is piecewise, these function pieces are continuous at all critical points with respect to the link parameters. Because altering the inequality in Line 1 from “less than” to “less than or equal to” does not change the solution. Hence, the Lipschitz continuity of the A-optimal design allocation (second part of Condition 1) is verified.

MLE Estimator for Link Parameters

The measurement observation at each link ℓ from the RI multicast follows a Bernoulli distribution with success probability μ_{ℓ} [De Andrade et al., 2023, Table II and Eq. (17)]. Hence, the maximum likelihood estimator (MLE) for the link parameter μ_{ℓ} is defined using the observations from all other RI multicast probes $m \in \mathcal{M} \setminus \{\ell\}$ as follows:

$$\hat{\mu}_{\ell} = \frac{\sum_{m \in \mathcal{M} \setminus \{\ell\}} A_{m,\ell}}{\sum_{m \in \mathcal{M} \setminus \{\ell\}} S_m}, \quad \text{for all links } \ell \in \mathcal{L}, \quad (10)$$

where we recall that S_m is the total number of qubits sent by probe m , and $A_{m,\ell}$ is the total number of qubits not flipped at link ℓ from the measurements of probe m . This estimator is unbiased.

Confidence Interval of MLE Estimator

By Hoeffding’s inequality, the confidence interval for the MLE estimator in (10) is given by, for some constant $C_2 > 0$, with a confidence level $1 - \delta$,

$$\mu_{\ell} \in \left(\hat{\mu}_{\ell} - C_2 \sqrt{\frac{\log \delta^{-1}}{\sum_{m \in \mathcal{M} \setminus \{\ell\}} S_m}}, \hat{\mu}_{\ell} + C_2 \sqrt{\frac{\log \delta^{-1}}{\sum_{m \in \mathcal{M} \setminus \{\ell\}} S_m}} \right), \quad \text{for all links } \ell \in \mathcal{L}.$$

Therefore, Condition 2 is verified with all $\gamma_{m,\ell} = \frac{1}{2}$ and thus $\gamma_{\min} = \frac{1}{2}$.

Regret of OPAL on the Bit-Flip Quantum Star Network with RI Multicast

With the Lipschitz continuity of the A-optimal design criterion and the finite confidence interval with $\gamma_{\min} = \frac{1}{2}$, we apply Theorem 1 to derive the regret of OPAL on the quantum star network with bit-flip quantum channels as follows,

$R_T = \text{tr } \mathbf{I}^{-1}(\boldsymbol{\mu}; \boldsymbol{\phi}_T) - \text{tr } \mathbf{I}^{-1}(\boldsymbol{\mu}; \boldsymbol{\phi}^*) \leq C \left(\frac{\log T}{\xi T} \right)^{\frac{1}{2}} + \alpha \xi$. Unlike the regret derivation in Section 5.1, we cannot cancel the second $\alpha \xi$ term by setting a constant input ξ in this quantum network tomography task. Because the A-optimal allocation in (9) inherently includes probes with a zero allocation ratio, i.e., $\phi_m^* = 0$ for some m , which necessitates that the second term remains non-zero. This aligns with the intuition that it is difficult for an algorithm to avoid performing these ineffective probes without knowledge of the exact link parameters a priori, leading to a regret (convergence rate) slower than $\tilde{O}(T^{-\gamma_{\min}})$.

By selecting $\xi = T^{-\frac{1}{3}}$, we obtain the worst-case convergence guarantee of OPAL on the quantum star network with bit-flip quantum channels under the RI multicast, expressed as,

$$R_T = \text{tr } \mathbf{I}^{-1}(\boldsymbol{\mu}; \boldsymbol{\phi}_T) - \text{tr } \mathbf{I}^{-1}(\boldsymbol{\mu}; \boldsymbol{\phi}^*) \leq O \left(\left(\frac{\log T}{T} \right)^{\frac{1}{3}} \right).$$

In this case study, we focus on the quantum multicast setting for the quantum star network. Currently, no quantum unicast probes have been devised, and we thus leave the verification of the unicast setting for future work.

6.2 Simulations for Quantum Network Tomography

This section reports the empirical performance of OPAL algorithm in a 3-link quantum bit-flip network tomography task. The set of probing experiments consists of all three root-independent (RI) multicast probes, each picking the end node of one link as the root node. The same three baselines as in Section 5.2 are considered, and other basic setups are the same as well. Figure 6 presents the six performance metrics of algorithms for bit-flip tomography in a 3-link quantum star networks. The results demonstrate the superior performance of OPAL in the quantum network tomography scenario and supports the same observations as stated in Section 5.2. For general topology quantum networks, there are no prior tomography methods in the literature. Therefore, the experiments for ER graphs, as conducted in Section 5.2, are not applicable here.

7 Conclusion

This paper introduces a novel and general online experimental design algorithm for network tomography, termed online probe allocation (OPAL). Theoretically, OPAL is the first algorithm to offer rigorous regret guarantees for network tomography. We establish these guarantees by identifying two critical conditions:

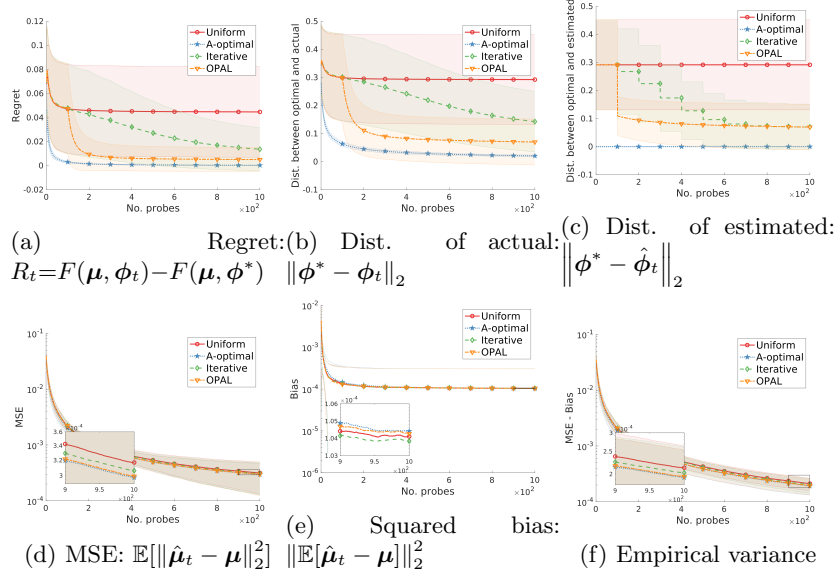


Figure 6: Comparison of algorithms for 3-link quantum star networks

Lipschitz continuity and confidence interval concentration. On the practical side, we validate these theoretical conditions in classical loss unicast networks and quantum bit-flip multicast networks, representing key use cases for network tomography. Empirically, we illustrate the superior performance of OPAL compared to existing methods in these two classical and quantum network tomography scenarios.

References

- Zeyuan Allen-Zhu, Yuanzhi Li, Aarti Singh, and Yining Wang. Near-optimal discrete optimization for experiment design: A regret minimization approach. *Mathematical Programming*, 186:439–478, 2021.
- P Auer. Finite-time analysis of the multiarmed bandit problem, 2002.
- Andrew Gehret Barto, Richard S Sutton, and CJCH Watkins. *Learning and sequential decision making*, volume 89. University of Massachusetts Amherst, MA, 1989.
- Tian Bu, Nick Duffield, Francesco Lo Presti, and Don Towsley. Network tomography on general topologies. *ACM SIGMETRICS Performance Evaluation Review*, 30(1):21–30, 2002.
- Ramón Cáceres, Nick G Duffield, Joseph Horowitz, and Don Towsley. Multicast-

- based inference of network-internal loss characteristics. *IEEE Transactions on Information theory*, 45(7):2462–2480, 1999.
- Wei Chen, Yajun Wang, and Siyu Yang. Efficient influence maximization in social networks. In *Proceedings of the 15th ACM SIGKDD international conference on Knowledge discovery and data mining*, pages 199–208, 2009.
- Wei Chen, Yajun Wang, and Yang Yuan. Combinatorial multi-armed bandit: General framework and applications. In *International conference on machine learning*, pages 151–159. PMLR, 2013.
- AHeroIII Coates, Alfred O Hero III, Robert Nowak, and Bin Yu. Internet tomography. *IEEE Signal processing magazine*, 19(3):47–65, 2002.
- Richard Combes, Stefan Magureanu, and Alexandre Proutiere. Minimal exploration in structured stochastic bandits. *Advances in Neural Information Processing Systems*, 30, 2017.
- Matheus Guedes De Andrade, Jaime Diaz, Jake Navas, Saikat Guha, Inès Montañó, Brian Smith, Michael Raymer, and Don Towsley. Quantum network tomography with multi-party state distribution. In *2022 IEEE International Conference on Quantum Computing and Engineering (QCE)*, pages 400–409. IEEE, 2022.
- Matheus Guedes De Andrade, Jake Navas, Inès Montañó, and Don Towsley. On the characterization of quantum flip stars with quantum network tomography. In *2023 IEEE International Conference on Quantum Computing and Engineering (QCE)*, volume 1, pages 1260–1270. IEEE, 2023.
- Matheus Guedes De Andrade, Jake Navas, Saikat Guha, Inès Montañó, Michael Raymer, Brian Smith, and Don Towsley. Quantum network tomography. *IEEE Network*, 2024.
- Nick G Duffield and F Lo Presti. Multicast inference of packet delay variance at interior network links. In *Proceedings IEEE INFOCOM 2000. Conference on Computer Communications. Nineteenth Annual Joint Conference of the IEEE Computer and Communications Societies (Cat. No. 00CH37064)*, volume 3, pages 1351–1360. IEEE, 2000.
- Xavier Fontaine, Pierre Perrault, Michal Valko, and Vianney Perchet. Online A-optimal design and active linear regression. In *International Conference on Machine Learning*, pages 3374–3383. PMLR, 2021.
- Xinzhe Fu and Eytan Modiano. Optimal routing to parallel servers with unknown utilities—multi-armed bandit with queues. *IEEE/ACM Transactions on Networking*, 31(5):1997–2012, 2022.
- Aurélien Garivier and Emilie Kaufmann. Optimal best arm identification with fixed confidence. In *Conference on Learning Theory*, pages 998–1027. PMLR, 2016.

- James Gilman, Laura Walls, Lucia Bandiera, and Filippo Menolascina. Statistical design of experiments for synthetic biology. *ACS synthetic biology*, 10(1):1–18, 2021.
- Abishek Gopalan and Srinivasan Ramasubramanian. On identifying additive link metrics using linearly independent cycles and paths. *IEEE/ACM Transactions on Networking*, 20(3):906–916, 2011.
- Yu Gu, Guofei Jiang, Vishal Singh, and Yueping Zhang. Optimal probing for unicast network delay tomography. In *2010 Proceedings IEEE INFOCOM*, pages 1–9. IEEE, 2010.
- Linda M Haines, Inna Perevovskaya, and William F Rosenberger. Bayesian optimal designs for phase i clinical trials. *Biometrics*, 59(3):591–600, 2003.
- Elad Hazan et al. Introduction to online convex optimization. *Foundations and Trends® in Optimization*, 2(3-4):157–325, 2016.
- Ting He, Chang Liu, Ananthram Swami, Don Towsley, Theodoros Salonidis, Andrei Iu Bejan, and Paul Yu. Fisher information-based experiment design for network tomography. *ACM SIGMETRICS Performance Evaluation Review*, 43(1):389–402, 2015.
- Ting He, Liang Ma, Ananthram Swami, and Don Towsley. *Network tomography: identifiability, measurement design, and network state inference*. Cambridge University Press, 2021.
- Branislav Kveton, Muhammad Jehangir Amjad, Christophe Diot, Dimitris Konomis, Augustin Soule, and Xiaolong Yang. Optimal probing with statistical guarantees for network monitoring at scale. *Computer Communications*, 192:119–131, 2022.
- Tor Lattimore and Csaba Szepesvári. *Bandit algorithms*. Cambridge University Press, 2020.
- Riccardo Leardi. Experimental design in chemistry: A tutorial. *Analytica chimica acta*, 652(1-2):161–172, 2009.
- Erich L Lehmann and George Casella. *Theory of point estimation*. Springer Science & Business Media, 2006.
- Lihong Li, Wei Chu, John Langford, and Robert E Schapire. A contextual-bandit approach to personalized news article recommendation. In *Proceedings of the 19th international conference on World wide web*, pages 661–670, 2010.
- F Lo Presti, Nick G Duffield, Joseph Horowitz, and Don Towsley. Multicast-based inference of network-internal delay distributions. *IEEE/ACM Transactions On Networking*, 10(6):761–775, 2002.
- Jesús López-Fidalgo. Optimal experimental design. *Lecture Notes in Statistics*, 226, 2023.

- Liang Ma, Ting He, Ananthram Swami, Don Towsley, Kin K Leung, and Jessica Lowe. Node failure localization via network tomography. In *Proceedings of the 2014 Conference on Internet Measurement Conference*, pages 195–208, 2014.
- Michael A Nielsen and Isaac L Chuang. *Quantum computation and quantum information*. Cambridge university press, 2010.
- Mícheál O’Searcoid. *Metric spaces*. Springer Science & Business Media, 2006.
- Friedrich Pukelsheim. *Optimal design of experiments*. SIAM, 2006.
- William R Thompson. On the likelihood that one unknown probability exceeds another in view of the evidence of two samples. *Biometrika*, 25(3-4):285–294, 1933.
- Yolanda Tsang, Mark Coates, and Robert D Nowak. Network delay tomography. *IEEE Transactions on Signal Processing*, 51(8):2125–2136, 2003.
- Bowei Xi, George Michailidis, and Vijayan N Nair. Estimating network loss rates using active tomography. *Journal of the American Statistical Association*, 101(476):1430–1448, 2006.

A Proofs of Lemmas 2 and 3

In this section, we provide the proofs of Lemmas 2 and 3.

Proof of Lemma 2. In this proof, we fix a link $\ell \in \mathcal{L}$ and omit its appearance in subscript for simplicity. Denote $\mathcal{M}^+ := \{m \in \mathcal{M} : \kappa_{\ell,m} > 0\}$ and $\mathcal{M}^- := \{m \in \mathcal{M} : \kappa_{\ell,m} < 0\}$ as the sets of probes with positive and negative entries in the inverse matrix \mathbf{Q}^{-1} 's ℓ^{th} column, respectively. Then, we have

$$\begin{aligned}
\hat{\mu}_\ell &= \prod_{m \in \mathcal{M}} \hat{\nu}_m^{\kappa_m} = \frac{\prod_{m \in \mathcal{M}^+} \hat{\nu}_m^{\kappa_m}}{\prod_{m \in \mathcal{M}^-} \hat{\nu}_m^{-\kappa_m}} \\
&\stackrel{(a)}{\leq} \frac{\prod_{m \in \mathcal{M}^+} (\nu_m + r_m)^{\kappa_m}}{\prod_{m \in \mathcal{M}^-} (\nu_m - r_m)^{-\kappa_m}} = \frac{\prod_{m \in \mathcal{M}^+} \nu_m^{\kappa_m}}{\prod_{m \in \mathcal{M}^-} \nu_m^{-\kappa_m}} \cdot \frac{\prod_{m \in \mathcal{M}^+} (1 + r_m/\nu_m)^{\kappa_m}}{\prod_{m \in \mathcal{M}^-} (1 - r_m/\nu_m)^{-\kappa_m}} \\
&\stackrel{(b)}{=} \mu_\ell \cdot \frac{\prod_{m \in \mathcal{M}^+} (1 + r'_m)^{\kappa_m}}{\prod_{m \in \mathcal{M}^-} (1 - r'_m)^{-\kappa_m}} = \mu_\ell + \mu_\ell \left(\frac{\prod_{m \in \mathcal{M}^+} (1 + r'_m)^{\kappa_m}}{\prod_{m \in \mathcal{M}^-} (1 - r'_m)^{-\kappa_m}} - 1 \right) \\
&= \mu_\ell + \mu_\ell \cdot \frac{\prod_{m \in \mathcal{M}^+} (1 + r'_m)^{2\kappa_m} - \prod_{m \in \mathcal{M}^-} (1 - r'_m)^{-2\kappa_m}}{\prod_{m \in \mathcal{M}^-} (1 - r'_m)^{-\kappa_m} (\prod_{m \in \mathcal{M}^+} (1 + r'_m)^{\kappa_m} + \prod_{m \in \mathcal{M}^-} (1 - r'_m)^{-\kappa_m})} \\
&\stackrel{(c)}{\leq} \mu_\ell + C \sum_{m \in \mathcal{M}^+ \cup \mathcal{M}^-} (r'_m)^{2\kappa'_m}, \quad \text{for some constant } C,
\end{aligned}$$

where inequality (a) is because $\nu_m \in (\hat{\nu}_m - r_m, \hat{\nu}_m + r_m)$ by the Hoeffding's inequality and $r_m := \sqrt{\frac{\log(\delta^{-1}/M)}{S_m}}$, equation (b) is due to $\mu_\ell = \prod_{m \in \mathcal{M}} \nu_m^{\kappa_m}$ when the MLE estimator has accurate inputs and denote $r'_m := r_m/\nu_m$, and inequality (c) is by noticing that (c1) for the nominator, $2\kappa_m \in \{1, 2\}, \forall m \in \mathcal{M}^+$ and $-2\kappa_m \in \{1, 2\}, \forall m \in \mathcal{M}^-$, and therefore, the nominator can be upper bounded by $O(\sum_{m \in \mathcal{M}^+ \cup \mathcal{M}^-} r'_m)$ while all other terms are with high orders can be omitted, and (c2) the denominator can be lower bounded by a constant when $S_m \geq O(\log T)$ for all $m \in \mathcal{M}$. \square

Proof of Lemma 3. Step 1. Block diagonalization. By row and column switch, one can transform matrix \mathbf{Q} to a block diagonal matrix, as follows,

$$\mathbf{Q} \longleftrightarrow \begin{bmatrix} \mathbf{Q}_1 & 0 & \dots & 0 \\ 0 & \mathbf{Q}_2 & \dots & 0 \\ \vdots & \vdots & \ddots & \vdots \\ 0 & 0 & \dots & \mathbf{Q}_H \end{bmatrix},$$

where each submatrix \mathbf{Q}_h is a square matrix that cannot be further block diagonalized.

Step 2. Determinant calculation. By Laplace expansion and Leibniz's equation, we show $\det(\mathbf{Q}_h) \in \{\pm 2\}$ for all $h = 1, \dots, H$.

For each row of the matrix \mathbf{Q}_h , as in a unicast star network, it contains only two 1 entries while others are all zero entries. If there exists a column c

in matrix \mathbf{Q}_h that only has one 1 entry in row r and all other entries are zero, then we apply the Laplace expansion on this single 1 entry, leading to

$$\det(\mathbf{Q}_h) = (-1)^{r+c} \det(\mathbf{Q}_{h,\text{sub},r,c}).$$

For the submatrix $\mathbf{Q}_{h,\text{sub},r,c}$, if there exists another column c' that only has one 1 entry, then we can apply the Laplace expansion on this single 1 entry again. By iteratively applying the Laplace expansion, we finally obtain a matrix \mathbf{Q}'_h with no single 1-entry column. As each row has exactly two 1 entries, no single 1-entry column also implies there is no column with more than two 1 entries. Therefore, \mathbf{Q}'_h is a square matrix with all columns and rows having exactly two 1 entries. Following the block diagonalization in Step 1, we also note that the matrix \mathbf{Q}'_h cannot be further decomposed into smaller block diagonal matrices, either.

Then, we apply the Leibniz's equation to calculate the determinant of \mathbf{Q}' as follows,

$$\det(\mathbf{Q}'_h) = \sum_{\sigma \in \text{perm.}} \text{sgn}(\sigma) \prod_{\ell=1}^L (\mathbf{Q}'_h)_{\ell, \sigma(\ell)},$$

where σ is a permutation of the column of the matrix \mathbf{Q}' , and $\text{sgn}(\sigma)$ is the sign of the permutation. Because each row has exactly two 1 entries and the matrix cannot be further decomposed, the Leibniz's equation only has two non-zero terms with value either 1 or -1 in the summation, and noticing the matrix is non-singular, the determinant is ± 2 .

Step 3. Submatrix inversion. Notice that for the block diagonal matrix, the inverse matrix is also block diagonalized, as follows,

$$\begin{bmatrix} \mathbf{Q}_1 & 0 & \dots & 0 \\ 0 & \mathbf{Q}_2 & \dots & 0 \\ \vdots & \vdots & \ddots & \vdots \\ 0 & 0 & \dots & \mathbf{Q}_H \end{bmatrix}^{-1} = \begin{bmatrix} \mathbf{Q}_1^{-1} & 0 & \dots & 0 \\ 0 & \mathbf{Q}_2^{-1} & \dots & 0 \\ \vdots & \vdots & \ddots & \vdots \\ 0 & 0 & \dots & \mathbf{Q}_H^{-1} \end{bmatrix}.$$

Hence, we only need to show that for each submatrix \mathbf{Q}_h , the inverse matrix \mathbf{Q}_h^{-1} only has $\{0, \pm\frac{1}{2}, \pm 1\}$ entries. As the inverse matrix \mathbf{Q}_h^{-1} can be calculated as follows,

$$\mathbf{Q}_h^{-1} = \frac{1}{\det(\mathbf{Q}_h)} \mathbf{C}_h^T,$$

where \mathbf{C}_h is the cofactor matrix of \mathbf{Q}_h . The entries of \mathbf{C}_h are the determinants of the submatrices of \mathbf{Q}_h , whose values are in $\{0, \pm 1, \pm 2\}$ by applying the Leibniz's equation. As $\det(\mathbf{Q}_h) = \pm 2$, the entries of \mathbf{Q}_h^{-1} are in $\{0, \pm\frac{1}{2}, \pm 1\}$. \square

B Additional Experiments: Impact of Lazy Update Batch Size

In this appendix, we present additional experiments to investigate the impact of the lazy updates on OPAL. Figures 8 and 9 illustrate the impact of the lazy

update batch size on OPAL, indicating that the performance of OPAL remains robust regardless of the chosen lazy update batch size. From this observation, when the computation cost is a concern, one can choose a larger lazy update batch size to reduce the number of updates while maintaining a relatively good performance.

C Calculation of the Biased CRB for Loss Tomography in 3-Link Classical Star Network

As illustrated in Section 5.2, the curve trend of subfigures (d) is different from that of subfigures (a), which is due to the biased MLE estimators (illustrated in subfigures (e)). This biased MLE breaks the equivalence between the MSE and MLE. In this section, we present the derivation of the biased CRB for the loss tomography in the classical 3-link star network.

C.1 Definition of the Biased Crame-Rao Lower Bound

We present a brief derivation of the general biased CRB for the a vector of biased estimator $\hat{\boldsymbol{\mu}}$ as follows,

$$\begin{aligned} \text{MSE}(\hat{\boldsymbol{\mu}}) &:= \begin{bmatrix} \mathbb{E}[(\hat{\mu}_1 - \mu_1)^2] & \mathbb{E}[(\hat{\mu}_1 - \mu_1)(\hat{\mu}_2 - \mu_2)] & \mathbb{E}[(\hat{\mu}_1 - \mu_1)(\hat{\mu}_3 - \mu_3)] \\ \mathbb{E}[(\hat{\mu}_2 - \mu_2)(\hat{\mu}_1 - \mu_1)] & \mathbb{E}[(\hat{\mu}_2 - \mu_2)^2] & \mathbb{E}[(\hat{\mu}_2 - \mu_2)(\hat{\mu}_3 - \mu_3)] \\ \mathbb{E}[(\hat{\mu}_3 - \mu_3)(\hat{\mu}_1 - \mu_1)] & \mathbb{E}[(\hat{\mu}_3 - \mu_3)(\hat{\mu}_2 - \mu_2)] & \mathbb{E}[(\hat{\mu}_3 - \mu_3)^2] \end{bmatrix} \\ &= \text{Cov}(\hat{\boldsymbol{\mu}}) + b(\hat{\boldsymbol{\mu}})b(\hat{\boldsymbol{\mu}})^T \\ &\succeq (\mathbf{I}(\boldsymbol{\mu}) + \mathbf{J}_b(\boldsymbol{\mu}))^{-1} + b(\hat{\boldsymbol{\mu}})b(\hat{\boldsymbol{\mu}})^T, \end{aligned}$$

where $\mathbf{J}_b(\boldsymbol{\mu}) := \left(\frac{\partial b(\boldsymbol{\mu})}{\partial \boldsymbol{\mu}} \right)^T \cdot \mathbf{I}(\boldsymbol{\mu}) \cdot \frac{\partial b(\boldsymbol{\mu})}{\partial \boldsymbol{\mu}}$, and $b(\boldsymbol{\mu}) = [\mathbb{E}[\hat{\mu}_1] - \mu_1, \mathbb{E}[\hat{\mu}_2] - \mu_2, \mathbb{E}[\hat{\mu}_3] - \mu_3]^T$ is the bias of the MLE estimator, and $\frac{\partial b(\boldsymbol{\mu})}{\partial \boldsymbol{\mu}}$ is the Jacobian matrix of $b(\boldsymbol{\mu})$ with respect to $\boldsymbol{\mu}$. Then, taking trace on both sides yields

$$\underbrace{\sum_{\ell=1}^L \mathbb{E}[(\hat{\mu}_\ell - \mu_\ell)^2]}_{\text{MSE}} \geq \underbrace{\text{tr} \left((\mathbf{I}(\boldsymbol{\mu}) + \mathbf{J}_b(\boldsymbol{\mu}))^{-1} \right)}_{\text{Biased CRB}} + \underbrace{\sum_{\ell=1}^L (\mathbb{E}[\hat{\mu}_\ell - \mu_\ell])^2}_{\text{Squared Bias}}$$

With the general definition of the biased CRB, i.e., $\text{tr} \left((\mathbf{I}(\boldsymbol{\mu}) + \mathbf{J}_b(\boldsymbol{\mu}))^{-1} \right)$, we then derive the specific form of Fisher information matrix $\mathbf{I}(\boldsymbol{\mu})$ and Jacobian matrix $\mathbf{J}(\boldsymbol{\mu})$ for the biased CRB of the for the loss tomography in the classical 3-link star network.

C.2 Specific form of the Fisher Information Matrix and the Jacobian matrix

The Fisher information matrix is given by

$$\mathbf{I}(\boldsymbol{\mu}; \mathbf{S}) = \begin{bmatrix} -\frac{S_1\mu_2}{\mu_1(\mu_1\mu_2-1)} - \frac{S_2\mu_3}{\mu_1(\mu_1\mu_3-1)} & -\frac{S_1}{\mu_1\mu_2-1} & -\frac{S_2}{\mu_1\mu_3-1} \\ -\frac{S_1}{\mu_1\mu_2-1} & -\frac{S_1\mu_1}{\mu_2(\mu_1\mu_2-1)} - \frac{S_3\mu_3}{\mu_2(\mu_2\mu_3-1)} & -\frac{S_3}{\mu_2\mu_3-1} \\ -\frac{S_2}{\mu_1\mu_3-1} & -\frac{S_3}{\mu_2\mu_3-1} & -\frac{S_2\mu_1}{\mu_3(\mu_1\mu_3-1)} - \frac{S_3\mu_2}{\mu_3(\mu_2\mu_3-1)} \end{bmatrix}$$

where the $\mathbf{S} := (S_1, S_2, S_3)$ are the number of samples in each unicast probe. This is slightly different from the $\mathbf{I}(\boldsymbol{\mu}; \boldsymbol{\phi})$ definition, where the $\boldsymbol{\phi} = \mathbf{S}/\sum_{\ell=1}^3 S_i$ is the allocation ratio. We use the \mathbf{S} notation because different from the linear property of FIM regarding the allocation times, the later matrix $\mathbf{J}_b(\boldsymbol{\mu}; \mathbf{S})$ is not linear with respect to the allocation times, and thus cannot be simplified to the $\mathbf{J}(\boldsymbol{\mu}; \boldsymbol{\phi})$ form as the FIM.

The matrix $\mathbf{J}_b(\boldsymbol{\mu}; \mathbf{S})$ is 3-by-3. Below, we present each element of the matrix $\mathbf{J}_b(\boldsymbol{\mu}; \mathbf{S})$ in detail.

$$\begin{aligned} \mathbf{J}_b(\boldsymbol{\mu}; \mathbf{S})_{1,1} &= \sum_{y_2=1}^{S_2} \left(\mu_1^{y_2-1} \mu_3^{y_2} y_2 \binom{S_2}{y_2} \left(\frac{S_2}{y_2} \right)^{\frac{1}{2}} (1 - \mu_1\mu_3)^{S_2-y_2} - \mu_1^{y_2} \mu_3 \mu_3^{y_2} \binom{S_2}{y_2} (S_2 - y_2) \left(\frac{S_2}{y_2} \right)^{\frac{1}{2}} (1 - \mu_1\mu_3)^{S_2-y_2-1} \right) \\ &\quad \times \sum_{y_1=1}^{S_1} \mu_2^{y_1} \mu_3^{y_1} \binom{S_1}{y_1} \left(\frac{S_1}{y_1} \right)^{\frac{1}{2}} (1 - \mu_2\mu_3)^{S_1-y_1} \times \sum_{y_3=1}^{S_3} \mu_1^{y_3} \mu_2^{y_3} \binom{S_3}{y_3} \left(\frac{S_3}{y_3} \right)^{\frac{1}{2}} (1 - \mu_1\mu_2)^{S_3-y_3} \\ &\quad + \sum_{y_3=1}^{S_3} \left(\mu_1^{y_3-1} \mu_2^{y_3} y_3 \binom{S_3}{y_3} \left(\frac{S_3}{y_3} \right)^{\frac{1}{2}} (1 - \mu_1\mu_2)^{S_3-y_3} - \mu_1^{y_3} \mu_2 \mu_2^{y_3} \binom{S_3}{y_3} (S_3 - y_3) \left(\frac{S_3}{y_3} \right)^{\frac{1}{2}} (1 - \mu_1\mu_2)^{S_3-y_3-1} \right) \\ &\quad \times \sum_{y_1=1}^{S_1} \mu_2^{y_1} \mu_3^{y_1} \binom{S_1}{y_1} \left(\frac{S_1}{y_1} \right)^{\frac{1}{2}} (1 - \mu_2\mu_3)^{S_1-y_1} \times \sum_{y_2=1}^{S_2} \mu_1^{y_2} \mu_3^{y_2} \binom{S_2}{y_2} \left(\frac{S_2}{y_2} \right)^{\frac{1}{2}} (1 - \mu_1\mu_3)^{S_2-y_2} - 1, \\ \mathbf{J}_b(\boldsymbol{\mu}; \mathbf{S})_{1,2} &= \sum_{y_1=1}^{S_1} \left(\mu_2^{y_1-1} \mu_3^{y_1} y_1 \binom{S_1}{y_1} \left(\frac{S_1}{y_1} \right)^{\frac{1}{2}} (1 - \mu_2\mu_3)^{S_1-y_1} - \mu_2^{y_1} \mu_3 \mu_3^{y_1} \binom{S_1}{y_1} (S_1 - y_1) \left(\frac{S_1}{y_1} \right)^{\frac{1}{2}} (1 - \mu_2\mu_3)^{S_1-y_1-1} \right) \\ &\quad \times \sum_{y_2=1}^{S_2} \mu_1^{y_2} \mu_3^{y_2} \binom{S_2}{y_2} \left(\frac{S_2}{y_2} \right)^{\frac{1}{2}} (1 - \mu_1\mu_3)^{S_2-y_2} \times \sum_{y_3=1}^{S_3} \mu_1^{y_3} \mu_2^{y_3} \binom{S_3}{y_3} \left(\frac{S_3}{y_3} \right)^{\frac{1}{2}} (1 - \mu_1\mu_2)^{S_3-y_3} \\ &\quad + \sum_{y_3=1}^{S_3} \left(\mu_1^{y_3} \mu_2^{y_3-1} y_3 \binom{S_3}{y_3} \left(\frac{S_3}{y_3} \right)^{\frac{1}{2}} (1 - \mu_1\mu_2)^{S_3-y_3} - \mu_1 \mu_1^{y_3} \mu_2^{y_3} \binom{S_3}{y_3} (S_3 - y_3) \left(\frac{S_3}{y_3} \right)^{\frac{1}{2}} (1 - \mu_1\mu_2)^{S_3-y_3-1} \right) \\ &\quad \times \sum_{y_1=1}^{S_1} \mu_2^{y_1} \mu_3^{y_1} \binom{S_1}{y_1} \left(\frac{S_1}{y_1} \right)^{\frac{1}{2}} (1 - \mu_2\mu_3)^{S_1-y_1} \times \sum_{y_2=1}^{S_2} \mu_1^{y_2} \mu_3^{y_2} \binom{S_2}{y_2} \left(\frac{S_2}{y_2} \right)^{\frac{1}{2}} (1 - \mu_1\mu_3)^{S_2-y_2}, \end{aligned}$$

$$\begin{aligned}
J_b(\mu; \mathbf{S})_{1,3} &= \sum_{y_1=1}^{S_1} \left(\mu_2^{y_1} \mu_3^{y_1-1} y_1 \binom{S_1}{y_1} \left(\frac{S_1}{y_1} \right)^{\frac{1}{2}} (1 - \mu_2 \mu_3)^{S_1-y_1} - \mu_2 \mu_2^{y_1} \mu_3^{y_1} \binom{S_1}{y_1} (S_1 - y_1) \left(\frac{S_1}{y_1} \right)^{\frac{1}{2}} (1 - \mu_2 \mu_3)^{S_1-y_1-1} \right) \\
&\quad \times \sum_{y_2=1}^{S_2} \mu_1^{y_2} \mu_3^{y_2} \binom{S_2}{y_2} \left(\frac{S_2}{y_2} \right)^{\frac{1}{2}} (1 - \mu_1 \mu_3)^{S_2-y_2} \times \sum_{y_3=1}^{S_3} \mu_1^{y_3} \mu_2^{y_3} \binom{S_3}{y_3} \left(\frac{S_3}{y_3} \right)^{\frac{1}{2}} (1 - \mu_1 \mu_2)^{S_3-y_3} \\
&\quad + \sum_{y_2=1}^{S_2} \left(\mu_1^{y_2} \mu_3^{y_2-1} y_2 \binom{S_2}{y_2} \left(\frac{S_2}{y_2} \right)^{\frac{1}{2}} (1 - \mu_1 \mu_3)^{S_2-y_2} - \mu_1 \mu_1^{y_2} \mu_3^{y_2} \binom{S_2}{y_2} (S_2 - y_2) \left(\frac{S_2}{y_2} \right)^{\frac{1}{2}} (1 - \mu_1 \mu_3)^{S_2-y_2-1} \right) \\
&\quad \times \sum_{y_1=1}^{S_1} \mu_2^{y_1} \mu_3^{y_1} \binom{S_1}{y_1} \left(\frac{S_1}{y_1} \right)^{\frac{1}{2}} (1 - \mu_2 \mu_3)^{S_1-y_1} \times \sum_{y_3=1}^{S_3} \mu_1^{y_3} \mu_2^{y_3} \binom{S_3}{y_3} \left(\frac{S_3}{y_3} \right)^{\frac{1}{2}} (1 - \mu_1 \mu_2)^{S_3-y_3}, \\
J_b(\mu; \mathbf{S})_{2,1} &= \sum_{y_2=1}^{S_2} \left(\mu_1^{y_2-1} \mu_3^{y_2} y_2 \binom{S_2}{y_2} \left(\frac{S_2}{y_2} \right)^{1/2} (1 - \mu_1 \mu_3)^{S_2-y_2} - \mu_1^{y_2} \mu_3 \mu_3^{y_2} \binom{S_2}{y_2} (S_2 - y_2) \left(\frac{S_2}{y_2} \right)^{1/2} (1 - \mu_1 \mu_3)^{S_2-y_2-1} \right) \\
&\quad \times \sum_{y_1=1}^{S_1} \mu_2^{y_1} \mu_3^{y_1} \binom{S_1}{y_1} \left(\frac{y_1}{S_1} \right)^{1/2} (1 - \mu_2 \mu_3)^{S_1-y_1} \times \sum_{y_3=1}^{S_3} \mu_1^{y_3} \mu_2^{y_3} \binom{S_3}{y_3} \left(\frac{y_3}{S_3} \right)^{1/2} (1 - \mu_1 \mu_2)^{S_3-y_3} \\
&\quad + \sum_{y_3=1}^{S_3} \left(\mu_1^{y_3-1} \mu_2^{y_3} y_3 \binom{S_3}{y_3} \left(\frac{y_3}{S_3} \right)^{1/2} (1 - \mu_1 \mu_2)^{S_3-y_3} - \mu_1^{y_3} \mu_2 \mu_2^{y_3} \binom{S_3}{y_3} (S_3 - y_3) \left(\frac{y_3}{S_3} \right)^{1/2} (1 - \mu_1 \mu_2)^{S_3-y_3-1} \right) \\
&\quad \times \sum_{y_1=1}^{S_1} \mu_2^{y_1} \mu_3^{y_1} \binom{S_1}{y_1} \left(\frac{y_1}{S_1} \right)^{1/2} (1 - \mu_2 \mu_3)^{S_1-y_1} \times \sum_{y_2=1}^{S_2} \mu_1^{y_2} \mu_3^{y_2} \binom{S_2}{y_2} \left(\frac{S_2}{y_2} \right)^{1/2} (1 - \mu_1 \mu_3)^{S_2-y_2}, \\
J_b(\mu; \mathbf{S})_{2,2} &= \sum_{y_1=1}^{S_1} \left(\mu_2^{y_1-1} \mu_3^{y_1} y_1 \binom{S_1}{y_1} \left(\frac{y_1}{S_1} \right)^{1/2} (1 - \mu_2 \mu_3)^{S_1-y_1} - \mu_2^{y_1} \mu_3 \mu_3^{y_1} \binom{S_1}{y_1} (S_1 - y_1) \left(\frac{y_1}{S_1} \right)^{1/2} (1 - \mu_2 \mu_3)^{S_1-y_1-1} \right) \\
&\quad \times \sum_{y_2=1}^{S_2} \mu_1^{y_2} \mu_3^{y_2} \binom{S_2}{y_2} \left(\frac{S_2}{y_2} \right)^{1/2} (1 - \mu_1 \mu_3)^{S_2-y_2} \times \sum_{y_3=1}^{S_3} \mu_1^{y_3} \mu_2^{y_3} \binom{S_3}{y_3} \left(\frac{y_3}{S_3} \right)^{1/2} (1 - \mu_1 \mu_2)^{S_3-y_3} \\
&\quad + \sum_{y_3=1}^{S_3} \left(\mu_1^{y_3} \mu_2^{y_3-1} y_3 \binom{S_3}{y_3} \left(\frac{y_3}{S_3} \right)^{1/2} (1 - \mu_1 \mu_2)^{S_3-y_3} - \mu_1 \mu_1^{y_3} \mu_2^{y_3} \binom{S_3}{y_3} (S_3 - y_3) \left(\frac{y_3}{S_3} \right)^{1/2} (1 - \mu_1 \mu_2)^{S_3-y_3-1} \right) \\
&\quad \times \sum_{y_1=1}^{S_1} \mu_2^{y_1} \mu_3^{y_1} \binom{S_1}{y_1} \left(\frac{y_1}{S_1} \right)^{1/2} (1 - \mu_2 \mu_3)^{S_1-y_1} \times \sum_{y_2=1}^{S_2} \mu_1^{y_2} \mu_3^{y_2} \binom{S_2}{y_2} \left(\frac{S_2}{y_2} \right)^{1/2} (1 - \mu_1 \mu_3)^{S_2-y_2} - 1,
\end{aligned}$$

$$\begin{aligned}
J_b(\mu; \mathbf{S})_{2,3} &= \sum_{y_1=1}^{S_1} \left(\mu_2^{y_1} \mu_3^{y_1-1} y_1 \binom{S_1}{y_1} \left(\frac{y_1}{S_1} \right)^{1/2} (1 - \mu_2 \mu_3)^{S_1-y_1} - \mu_2 \mu_2^{y_1} \mu_3^{y_1} \binom{S_1}{y_1} (S_1 - y_1) \left(\frac{y_1}{S_1} \right)^{1/2} (1 - \mu_2 \mu_3)^{S_1-y_1-1} \right) \\
&\quad \times \sum_{y_2=1}^{S_2} \mu_1^{y_2} \mu_3^{y_2} \binom{S_2}{y_2} \left(\frac{S_2}{y_2} \right)^{1/2} (1 - \mu_1 \mu_3)^{S_2-y_2} \times \sum_{y_3=1}^{S_3} \mu_1^{y_3} \mu_2^{y_3} \binom{S_3}{y_3} \left(\frac{y_3}{S_3} \right)^{1/2} (1 - \mu_1 \mu_2)^{S_3-y_3} \\
&\quad + \sum_{y_2=1}^{S_2} \left(\mu_1^{y_2} \mu_3^{y_2-1} y_2 \binom{S_2}{y_2} \left(\frac{S_2}{y_2} \right)^{1/2} (1 - \mu_1 \mu_3)^{S_2-y_2} - \mu_1 \mu_1^{y_2} \mu_3^{y_2} \binom{S_2}{y_2} (S_2 - y_2) \left(\frac{S_2}{y_2} \right)^{1/2} (1 - \mu_1 \mu_3)^{S_2-y_2-1} \right) \\
&\quad \times \sum_{y_1=1}^{S_1} \mu_2^{y_1} \mu_3^{y_1} \binom{S_1}{y_1} \left(\frac{y_1}{S_1} \right)^{1/2} (1 - \mu_2 \mu_3)^{S_1-y_1} \times \sum_{y_3=1}^{S_3} \mu_1^{y_3} \mu_2^{y_3} \binom{S_3}{y_3} \left(\frac{y_3}{S_3} \right)^{1/2} (1 - \mu_1 \mu_2)^{S_3-y_3}, \\
J_b(\mu; \mathbf{S})_{3,1} &= \sum_{y_2=1}^{S_2} \left(\mu_1^{y_2-1} \mu_3^{y_2} y_2 \binom{S_2}{y_2} \left(\frac{y_2}{S_2} \right)^{1/2} (1 - \mu_1 \mu_3)^{S_2-y_2} - \mu_1^{y_2} \mu_3 \mu_3^{y_2} \binom{S_2}{y_2} (S_2 - y_2) \left(\frac{y_2}{S_2} \right)^{1/2} (1 - \mu_1 \mu_3)^{S_2-y_2-1} \right) \\
&\quad \times \sum_{y_1=1}^{S_1} \mu_2^{y_1} \mu_3^{y_1} \binom{S_1}{y_1} \left(\frac{y_1}{S_1} \right)^{1/2} (1 - \mu_2 \mu_3)^{S_1-y_1} \times \sum_{y_3=1}^{S_3} \mu_1^{y_3} \mu_2^{y_3} \binom{S_3}{y_3} \left(\frac{S_3}{y_3} \right)^{1/2} (1 - \mu_1 \mu_2)^{S_3-y_3} \\
&\quad + \sum_{y_3=1}^{S_3} \left(\mu_1^{y_3-1} \mu_2^{y_3} y_3 \binom{S_3}{y_3} \left(\frac{S_3}{y_3} \right)^{1/2} (1 - \mu_1 \mu_2)^{S_3-y_3} - \mu_1^{y_3} \mu_2 \mu_2^{y_3} \binom{S_3}{y_3} (S_3 - y_3) \left(\frac{S_3}{y_3} \right)^{1/2} (1 - \mu_1 \mu_2)^{S_3-y_3-1} \right) \\
&\quad \times \sum_{y_1=1}^{S_1} \mu_2^{y_1} \mu_3^{y_1} \binom{S_1}{y_1} \left(\frac{y_1}{S_1} \right)^{1/2} (1 - \mu_2 \mu_3)^{S_1-y_1} \times \sum_{y_2=1}^{S_2} \mu_1^{y_2} \mu_3^{y_2} \binom{S_2}{y_2} \left(\frac{y_2}{S_2} \right)^{1/2} (1 - \mu_1 \mu_3)^{S_2-y_2}, \\
J_b(\mu; \mathbf{S})_{3,2} &= \sum_{y_1=1}^{S_1} \left(\mu_2^{y_1-1} \mu_3^{y_1} y_1 \binom{S_1}{y_1} \left(\frac{y_1}{S_1} \right)^{1/2} (1 - \mu_2 \mu_3)^{S_1-y_1} - \mu_2^{y_1} \mu_3 \mu_3^{y_1} \binom{S_1}{y_1} (S_1 - y_1) \left(\frac{y_1}{S_1} \right)^{1/2} (1 - \mu_2 \mu_3)^{S_1-y_1-1} \right) \\
&\quad \times \sum_{y_2=1}^{S_2} \mu_1^{y_2} \mu_3^{y_2} \binom{S_2}{y_2} \left(\frac{y_2}{S_2} \right)^{1/2} (1 - \mu_1 \mu_3)^{S_2-y_2} \times \sum_{y_3=1}^{S_3} \mu_1^{y_3} \mu_2^{y_3} \binom{S_3}{y_3} \left(\frac{S_3}{y_3} \right)^{1/2} (1 - \mu_1 \mu_2)^{S_3-y_3} \\
&\quad + \sum_{y_3=1}^{S_3} \left(\mu_1^{y_3} \mu_2^{y_3-1} y_3 \binom{S_3}{y_3} \left(\frac{S_3}{y_3} \right)^{1/2} (1 - \mu_1 \mu_2)^{S_3-y_3} - \mu_1 \mu_1^{y_3} \mu_2^{y_3} \binom{S_3}{y_3} (S_3 - y_3) \left(\frac{S_3}{y_3} \right)^{1/2} (1 - \mu_1 \mu_2)^{S_3-y_3-1} \right) \\
&\quad \times \sum_{y_1=1}^{S_1} \mu_2^{y_1} \mu_3^{y_1} \binom{S_1}{y_1} \left(\frac{y_1}{S_1} \right)^{1/2} (1 - \mu_2 \mu_3)^{S_1-y_1} \times \sum_{y_2=1}^{S_2} \mu_1^{y_2} \mu_3^{y_2} \binom{S_2}{y_2} \left(\frac{y_2}{S_2} \right)^{1/2} (1 - \mu_1 \mu_3)^{S_2-y_2},
\end{aligned}$$

$$\begin{aligned}
J_b(\boldsymbol{\mu}; \mathbf{S})_{3,3} = & \sum_{y_1=1}^{S_1} \left(\mu_2^{y_1} \mu_3^{y_1-1} y_1 \binom{S_1}{y_1} \left(\frac{y_1}{S_1} \right)^{1/2} (1 - \mu_2 \mu_3)^{S_1-y_1} - \mu_2 \mu_2^{y_1} \mu_3^{y_1} \binom{S_1}{y_1} (S_1 - y_1) \left(\frac{y_1}{S_1} \right)^{1/2} (1 - \mu_2 \mu_3)^{S_1-y_1-1} \right) \\
& \times \sum_{y_2=1}^{S_2} \mu_1^{y_2} \mu_3^{y_2} \binom{S_2}{y_2} \left(\frac{y_2}{S_2} \right)^{1/2} (1 - \mu_1 \mu_3)^{S_2-y_2} \times \sum_{y_3=1}^{S_3} \mu_1^{y_3} \mu_2^{y_3} \binom{S_3}{y_3} \left(\frac{S_3}{y_3} \right)^{1/2} (1 - \mu_1 \mu_2)^{S_3-y_3} \\
& + \sum_{y_2=1}^{S_2} \left(\mu_1^{y_2} \mu_3^{y_2-1} y_2 \binom{S_2}{y_2} \left(\frac{y_2}{S_2} \right)^{1/2} (1 - \mu_1 \mu_3)^{S_2-y_2} - \mu_1 \mu_1^{y_2} \mu_3^{y_2} \binom{S_2}{y_2} (S_2 - y_2) \left(\frac{y_2}{S_2} \right)^{1/2} (1 - \mu_1 \mu_3)^{S_2-y_2-1} \right) \\
& \times \sum_{y_1=1}^{S_1} \mu_2^{y_1} \mu_3^{y_1} \binom{S_1}{y_1} \left(\frac{y_1}{S_1} \right)^{1/2} (1 - \mu_2 \mu_3)^{S_1-y_1} \times \sum_{y_3=1}^{S_3} \mu_1^{y_3} \mu_2^{y_3} \binom{S_3}{y_3} \left(\frac{S_3}{y_3} \right)^{1/2} (1 - \mu_1 \mu_2)^{S_3-y_3} - 1.
\end{aligned}$$

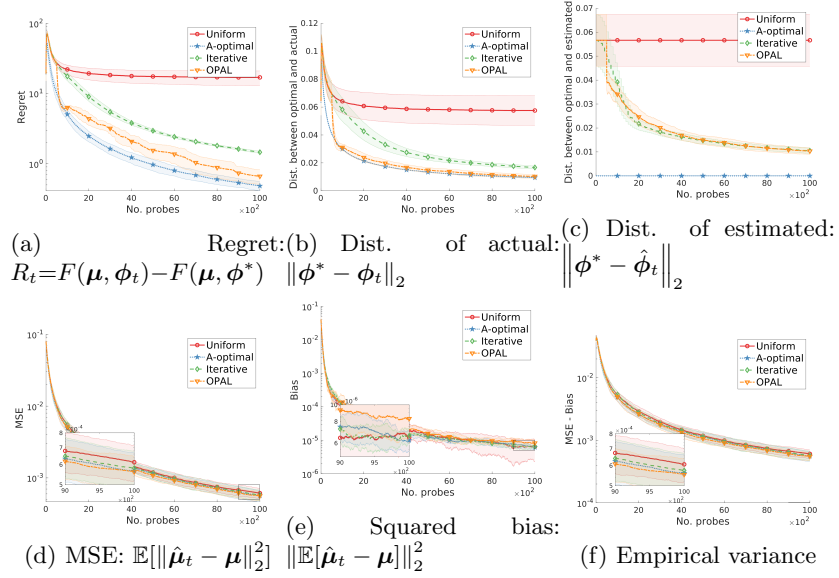


Figure 7: Comparison of algorithms for 30-link star networks

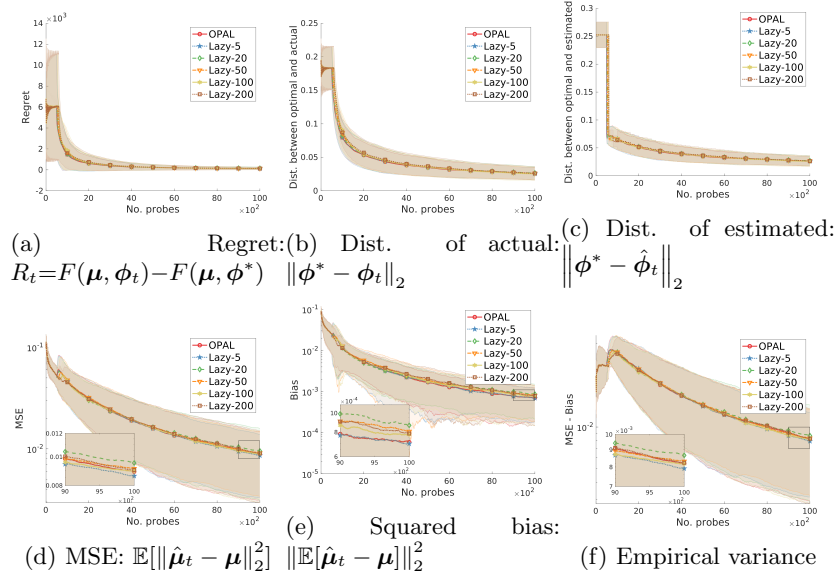


Figure 8: Impact of lazy update batch size on OPAL in loss tomography in classical ER network (zero initial sampling)

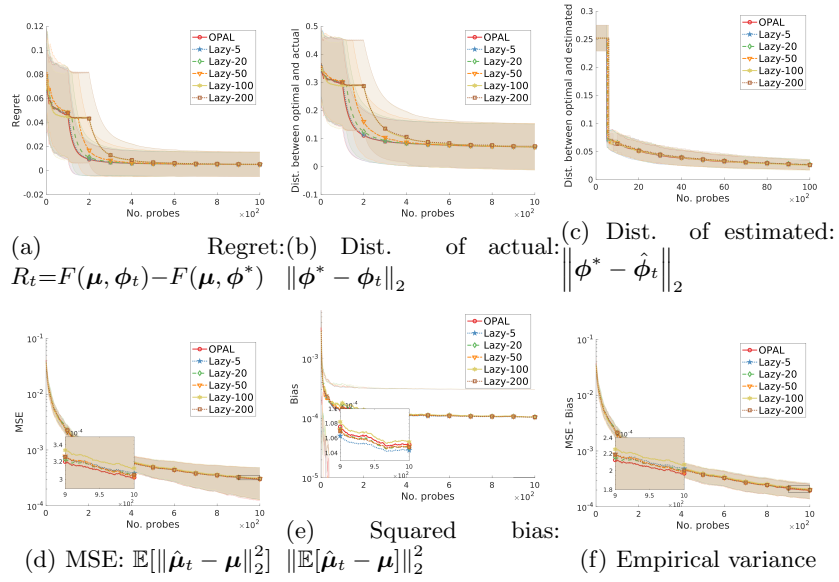


Figure 9: Impact of lazy update batch size on OPAL in bit-flip tomography in quantum 3-link star network (5% initial sampling)